

## ABSTRACT

SUSSMAN, RACHEL JO. Alterations in DOM Composition from Terminus to Coast: Matanuska Glacier to the Gulf of Alaska (Under the direction of Dr. Carli Arendt).

Glaciers feeding into the Gulf of Alaska (GOA) are rapidly retreating with poorly quantified effects on the downstream coastal ecosystems that rely on them. Dissolved organic matter (DOM) underlies the marine food web, yet no studies to date have captured longitudinal variations in DOM in Alaskan proglacial streams feeding the GOA. To better understand the transport of glacial nutrients to the ocean, we sought to characterize changes in DOM composition in the proglacial Matanuska River (MR) as it flows from the terminus of the Matanuska Glacier in southcentral Alaska (SC AK), through the proglacial Knik-Turnagain Arm (KTA) estuary system, to the central Cook Inlet (CCI) in the GOA. Using bulk nutrient, optical, and stable carbon isotopic analysis, we examined DOM sources and dynamics in the near-terminus MR and the KTA estuary. Additionally, we compared original % protein-like DOM (%P-DOM) in the near-terminus MR and nearby proglacial rivers to published %P-DOM of proglacial rivers in the Himalayas, SC AK, and Southeast Alaska (SE AK). %P-DOM significantly decreased over the first 11 km of the MR, likely driven by both microbial consumption of labile proteinaceous DOM and lateral additions of humic-like DOM from non-glacial tributaries. Our comparison between glacial environments yielded preliminary regional trends in the rate of %P-DOM decrease during transit that might be influenced by environmental differences between regions. In the KTA estuary we found that DOM inputs from surrounding wetlands, intertidal mudflats, CCI, and internal production overrode the signature of DOM from proglacial tributaries. Our findings verify rapid degradation of P-DOM in a proglacial river in Alaska, emphasize the need for further longitudinal research in proglacial rivers and estuaries, and suggest regionally specific trends in %P-DOM in proglacial rivers. As glaciers continue to retreat from the GOA due to climate change, less highly labile P-DOM will be delivered to the ocean by proglacial rivers with poorly quantified impacts on downstream ecosystems.

© Copyright 2021 by Rachel Jo Sussman

All Rights Reserved

Alterations in DOM Composition from Terminus to Coast: Matanuska Glacier to the Gulf of  
Alaska

by  
Rachel Jo Sussman

A thesis submitted to the Graduate Faculty of  
North Carolina State University  
in partial fulfillment of the  
requirements for the degree of  
Master of Science

Marine, Earth, and Atmospheric Sciences

Raleigh, North Carolina  
2021

APPROVED BY:

---

Dr. Carli A. Arendt  
Committee Chair

---

Dr. Astrid Schnetzer

---

Dr. Christopher L. Osburn

## **BIOGRAPHY**

I was born and raised in Claremont, California. I received my bachelor's degree in environmental science from Colorado College in 2016. After graduation, I worked a variety of jobs: field technician at the UC Davis Bodega Marine Laboratory in California; kayak guide in Juneau, Alaska; sustainability coordinator for the City of Whitefish, Montana; backcountry trail worker in the southwestern United States; and REI action sports specialist in California. In 2019, I headed east and joined the master's program in Marine, Earth, and Atmospheric Sciences at North Carolina State University in Raleigh, North Carolina.

## ACKNOWLEDGMENTS

This research was completed with funding from the Southeast Climate Adaptation Science Center at NCSU. I would like to thank my advisor, Dr. Carli Arendt, for her understanding and support as I endeavored to complete my degree and research during an incredibly difficult period in history. Thank you to Dr. Chris Osburn and Dr. Astrid Schnetzer for their insight and assistance. I would like to thank Rachael McCaully and Sailaja Pappala for their help and friendship in the field and in Raleigh. Additional thanks to Sarah Aarons for her field assistance. Thank you to Jacob Rudolph, Stephen Richardson, and the members of the Environmental and Agricultural Testing Services for their assistance with sample analysis. I would like to thank my friends and family, especially my mom, for their love, support, and wit throughout a wild two years (and the preceding 25 wild years). Gumbo and Fry, my two cats and COVID-coworkers, cannot be thanked enough for their highly refined lap-warming skills. Thank you to my dog, Okra, who constantly did his best to distract me from my work and brighten my day. And, most of all, thank you to Dr. Emily Reed, my pandemic survival partner, in-house statistician, figure whiz, formatting enthusiast, grad school mentor, pet co-parent, best friend, and girlfriend.

## TABLE OF CONTENTS

LIST OF TABLES .....	vii
LIST OF FIGURES .....	ix
<b>1.0. INTRODUCTION</b> .....	1
1.1. DOM in Glacial Systems .....	1
1.2. Glacial DOM in Coastal Ecosystems .....	3
1.3. Study Objective .....	4
<b>2.0. STUDY LOCATION</b> .....	5
2.1. Matanuska River .....	5
2.2. Knik/Turnagain Arm Estuary .....	5
2.3. Central Cook Inlet .....	7
<b>3.0. METHODS</b> .....	7
3.1. Sample Collection .....	7
3.2. In Situ Measurements .....	8
3.3. Bulk Nutrient Analysis .....	8
3.4. Optical Analysis .....	9
3.5. Stable Carbon Isotope Analyses .....	11
3.6. Comparative Data .....	11
3.7. Statistical Methods .....	12
<b>4.0. RESULTS</b> .....	12
4.1. Near-Terminus Matanuska River: 0-11 km .....	13
4.2. Knik/Turnagain Arm (KTA) Estuary .....	14
4.3. Riverine Endmembers .....	15
4.4. Central Cook Inlet (CCI) .....	15
4.5. Differences between Systems .....	16
4.6. Near-Terminus Cross-Study Comparison .....	16
<b>5.0. DISCUSSION</b> .....	17
5.1. Percent Protein-Like DOM from Terminus to 11 km .....	17
5.2. Interstudy Near-Terminus Comparison .....	21
5.3. Estuarine DOM Dynamics .....	25
<b>6.0. CONCLUSIONS</b> .....	28
<b>7.0. TABLES</b> .....	30
<b>8.0. FIGURES</b> .....	50
<b>9.0. REFERENCES</b> .....	68

**LIST OF TABLES**

Table 1 Descriptions of location abbreviations used..... 30

Table 2 Summary of fluorescence peaks and properties..... 31

Table 3 Summary of major optical parameters excluding fluorescence peaks ..... 32

Table 4 Linear model parameters for near-terminus environmental, DOM, and inorganic nutrient variables ..... 33

Table 5 Major nutrient species in the near-terminus Matanuska River ..... 34

Table 6 Near-terminus fluorescence data..... 35

Table 7 %P-DOM in the near-terminus Matanuska River..... 36

Table 8 Average  $\delta^{13}\text{C}$ -DOC and C/N for the near-terminus Matanuska River, riverine endmembers, Knik/Turnagain Arms estuary, and Central Cook Inlet..... 37

Table 9 DOM properties of the Hicks Creek confluence..... 38

Table 10 Nutrients for Knik/Turnagain Arms estuary in order of increasing salinity..... 39

Table 11 Linear model parameter estimates for estuarine system variables and salinity..... 40

Table 12 Optimal properties for Knik/Turnagain Arms estuary in order of increasing salinity..... 41

Table 13 Major nutrient concentrations for riverine endmembers feeding the Knik/Turnagain Arms estuary..... 42

Table 14 DOM parameters for riverine endmembers of the Knik/Turnagain Arms estuary..... 43

Table 15 Notable nutrients of Central Cook Inlet at 5 and 30m depths ..... 44

Table 16 Notable optical properties of Central Cook Inlet at 5 and 30m depths ..... 45

Table 17 ANOVA and Tukey HSD tests indicated that the Knik/Turnagain Arms estuary is elevated in the listed parameters relative to the riverine endmember..... 46

Table 18 Tukey HSD tests indicated that the Knik/Turnagain Arms estuary is elevated in the listed parameters relative to the Central Cook Inlet ..... 47

Table 19 Near-terminus cross-study comparison location and sampling information..... 48

Table 20	Linear model parameters for near-terminus cross-study comparison of %P-DOM and distance .....	49
----------	---	----

## LIST OF FIGURES

Figure 1	Map of the Matanuska Glacier system in South Central Alaska .....	50
Figure 2	Cook Inlet model topography .....	51
Figure 3	Near-terminus environmental parameters over the initial 11 km transect .....	52
Figure 4	$\text{NO}_3^-$ tends to increase over the 11 km near-terminus transect .....	53
Figure 5	Fluorescence peaks versus distance from terminus for near-terminus DOM.....	54
Figure 6	HIX and BIX versus distance from the terminus.....	55
Figure 7	%P-DOM vs distance from terminus .....	56
Figure 8	$\delta^{13}\text{C}$ versus C/N with corresponding DOM source materials in shaded boxes .....	57
Figure 9	$\delta^{13}\text{C}$ versus $\text{SUVA}_{254}$ for the Matanuska Glacier system.....	58
Figure 10	Trends between environmental, nutrient, and optical parameters and salinity in Knik/Turnagain Arms estuary.....	59
Figure 11	Boxplot of the range and median for $\text{NO}_3^-$ .....	60
Figure 12	Boxplot of DOC .....	61
Figure 13	Boxplots of humic-like peak A, peak C, and peak M .....	62
Figure 14	Boxplot of peak N .....	63
Figure 15	Boxplot of HIX .....	64
Figure 16	Boxplot of $\text{SUVA}_{254}$ .....	65
Figure 17	Boxplot of %P-DOM.....	66
Figure 18	Combined %P-DOM versus distance from glacial termini.....	67

## 1.0. INTRODUCTION

Rising atmospheric temperatures are rapidly depleting Alaska's glaciers. These glaciers are losing mass at among the highest rates on Earth, approximately  $75 \pm 11 \text{ Gt yr}^{-1}$ , with poorly quantified impacts on downstream ecosystems (Larsen et al., 2015). The Gulf of Alaska (GOA) in southern Alaska is heavily influenced by glacial runoff: twice as much freshwater discharge enters the GOA as the Mississippi River Delta delivers to the northern Gulf of Mexico, and almost half of that comes from melting glaciers (Neal, Hood, & Smikrud, 2010). The GOA is known for the bountiful fisheries along its continental shelf, which support a \$1.2 billion commercial fishing industry, subsistence and recreational fishers, and diverse wildlife (McDowell Group, 2017). At the base of the lucrative GOA food web are microbes that are adapted to rely on the substantial inputs of labile dissolved organic matter (DOM) in glacial runoff (Etherington et al., 2007; Fellman et al., 2010a). As climate change diminishes SC AK glaciers at accelerating rates, scientists must seek to understand how subsequent alterations in the DOM composition of glacial runoff will alter the GOA's ecology.

### 1.1. DOM in Glacial Systems

Glacial runoff contains dissolved organic carbon (DOC), nitrogen (DON), phosphorus (DOP), and other essential nutrients that fuel downstream microbial activity. Together, these constituents comprise DOM. DOC is a useful stand-in for DOM because it is easily measured and accounts for more than 50% of DOM, and the terms are often used interchangeably (Moody & Worrall, 2017). Glaciers were once thought to be devoid of nutrients due to harsh environments and minimal external inputs. In recent decades, however, scientists realized that glaciers were exporting small concentrations of DOM (Barker et al., 2006). Reported DOC in Alaskan non-glacial rivers ranges from  $2.2 - 8.0 \text{ mg L}^{-1}$ , while DOC in glacial rivers ranges from  $0.4 - 2.5 \text{ mg L}^{-1}$  (Fellman et al., 2014; Hood et al., 2009). Despite its low DOC content, glacial runoff has significant impacts on downstream ecosystems because of the massive quantity of overall runoff released (Hood et al., 2009). The GOA receives  $0.13 \pm 0.01 \text{ Tg}$  ( $1 \text{ Tg} = 10^{12} \text{ g}$ ) of glacially derived DOC each year (Hood & Scott, 2008). Glacial runoff into the GOA is expected to increase as the climate continues to warm (Neal et al., 2010), and it is unclear how DOM transport and composition will shift in response.

Even with the low levels of DOM typical in glacial runoff, the source and composition of glacial DOM has important implications for its ability to stimulate downstream production (Barker et al., 2006, 2013; Dubnick et al., 2010; Hood et al., 2009). DOM is an essential component of aquatic ecosystems and a biogeochemical link between terrestrial, riverine, and marine systems. In many rivers, DOM is largely derived from terrestrial plant matter that has been chemically reworked, incorporated into the soil, and then flushed into rivers (Hood et al., 2009). In glacial systems, however, recent glacial scouring leaves little soil organic matter (OM) remaining for export to proglacial rivers, or rivers flowing from glacial termini. The primary sources of DOM in proglacial streams are microbial communities in supraglacial (on top of the glacier) and subglacial (beneath the glacier) systems (Dubnick et al., 2010; Singer et al., 2012).

Supraglacial and subglacial ecosystems harbor pockets of intense microbial activity that ultimately contribute to DOM in proglacial streams and subsequent downstream ecosystems (Hood et al., 2009; Telling et al., 2010). Access to sunlight, liquid water, and windblown nutrients from dust create a hospitable environment for specialized microbes deposited on the glacial surface (Ren et al., 2019). Some of these microbes percolate through the ice and are introduced to the subglacial environment (Hotaling et al., 2017). Although there are limited external inputs and no sunlight in subglacial systems, some microorganisms can survive in subglacial water via chemosynthesis and the use of the little remaining ancient OM in glaciated soils and sediments (Hotaling et al., 2017; Singer et al., 2012). When supra- and subglacial runoff is released into a proglacial stream, it is enriched in proteinaceous DOM from these populations (Barker et al., 2013; Hotaling et al., 2017).

DOM in proglacial streams tends to be more bioavailable than that of non-glacial streams (Fellman et al., 2010a; Hood et al., 2009). DOM is a general term that encompasses OM with diverse chemical compositions, sizes, sources, and thus bioavailability as a microbial food source. DOM originates in the cells of living organisms and is microbially or photochemically degraded upon release (Bianchi, 2007). Freshly produced DOM is rich in highly labile substances such as proteins that are quickly decomposed. The remaining DOM can be converted into more recalcitrant humic substances, which are materials derived from the decay of plant and microbial remains. Microbial DOM has a much higher protein content than soil DOM, which is enriched in humic substances, cellulose, and lignin from plants (Bianchi, 2007; Fellman et al., 2008). Therefore, the protein-rich proglacial DOM tends to be highly labile.

Studies have demonstrated the proteinaceous composition and lability of proglacial stream DOM relative to non-glacial stream DOM using a combination of fluorescence spectroscopy, microbial incubations, and molecular techniques (e.g., Fellman et al., 2010a; Hood et al., 2009; Singer et al., 2012; Zhou et al., 2019). In a range of lowly to highly glaciated watersheds throughout southeastern and southcentral Alaska (SE AK and SC AK, respectively), Hood et al. (2009) and Fellman (2010a) found that the percent bioavailable DOC (%BDOC) was strongly correlated with both watershed glacier coverage and percent protein DOM (termed “%P-DOM” for the remainder of this study). In three unglaciated watersheds near Juneau, AK, %P-DOM averaged ~5.4%, while the most glaciated watershed had ~77% P-DOM (Fellman et al., 2010a; Hood et al., 2009). Studies on glacial systems throughout the world have found that near-terminus runoff is significantly enriched in PDOM and provides bioavailable nutrients to downstream ecosystems (Barker et al., 2006; Dubnick et al., 2010; Zhou et al., 2019).

## **1.2. Glacial DOM in Coastal Ecosystems**

The fate of glacial DOM and coastal organisms are closely intertwined in the GOA (Arimitsu et al., 2018; Fellman et al., 2015). In the highly productive GOA, coastal phytoplankton support the food web and rely heavily on external DOM inputs (Strom et al., 2016). The proteinaceous nature of glacially derived DOM facilitates its consumption by aquatic microbes and incorporation throughout the food web. Inoculation experiments using proglacial river and coastal microbes have found that glacial stream DOM is highly bioavailable compared to DOM from non-glacial streams, particularly to coastal phytoplankton (Fellman et al., 2010a; Hood et al., 2009; Singer et al., 2012). Stable ( $\delta^{13}\text{C}$ ,  $\delta^{15}\text{N}$ , and  $\delta^2\text{H}$ ) and radiogenic ( $\Delta^{14}\text{C}$ ) isotopic analysis of tissue and gut samples from various organisms have found evidence of glacial DOM incorporation through a range of trophic levels, including aquatic macroinvertebrates, juvenile salmonids, terrestrial spiders and beetles, and coastal birds, supporting its significance in proglacial ecosystems (Arimitsu et al., 2018; Fellman et al., 2015; Hågvar & Ohlson, 2013).

Estuaries are essential intermediaries in the transport of DOM between proglacial rivers and the GOA. They simultaneously affect and are affected by marine and riverine systems. Alaskan estuaries serve as protected wintering, breeding, nursery, and feeding grounds for various organisms, including many threatened migratory birds and anadromous fish such as salmon that continue up tributary rivers to spawning habitats (Etherington et al., 2007). Biogeochemical

processes in estuaries control the export of nutrients from terrestrial to marine systems. These estuarine processes are driven by riverine and marine inputs. In the GOA, where recent glaciation carved long, deep valleys, most estuaries are fjords that have been filled with glacially derived sediment (Etherington et al., 2007). Fjords in southern Alaska are complex systems that are influenced by the large tidal flux of the GOA and abundant fresh-water runoff from melting glaciers, as well as inputs from surrounding terrestrial systems (Etherington et al., 2007; Fellman et al., 2010a). The DOM in these contributions can be transformed by microbial metabolism, photochemical degradation, and physicochemical transformations, such as flocculation (Fellman et al., 2010b). The characteristics of DOM addition, loss, and transformation in estuaries impacts the abundance and composition of DOM delivered to the GOA with implications for coastal microbial production (Etherington et al., 2007; Fellman et al., 2010a). Research investigating these estuarine dynamics in the GOA is essential to understanding the flux of carbon from glaciers to gulf and potential downstream impacts on GOA ecosystems, including nutrient limitation, microbial community shifts, and subsequent changes in primary productivity.

### **1.3. Study Objectives**

The high turbidity and relatively short reaches of glacial rivers feeding the GOA has suggested that there is negligible removal of glacial DOC during transit to the ocean (Hood & Scott, 2008). The large amount of bioavailable DOM released from glaciers surrounding the GOA is assumed to sustain and nourish the region's substantial marine productivity with minimal losses to in-stream processes. Few studies have explored potential transformations of glacial DOM as it journeys from glacial termini to the ocean because proglacial streams are often viewed as direct conduits between systems with limited loss during transport. However, a few recent studies have found substantial changes in DOM compositions while moving downstream from glacial headwaters in Iceland (Chiffard et al., 2019) and the Himalayas (Zhou et al., 2019), with notable losses of proteinaceous material.

We investigated in-stream and estuarine alterations in DOM composition downstream of the glacial terminus in an Alaskan coastal glacial system. We sought to determine if the highly labile, glacially sourced DOM reached the GOA or was lost during transit. We used spectroscopic, bulk nutrient, and stable isotopic analysis to characterize the biogeochemical transformations of glacial runoff in the proglacial river and estuary. Our analysis yields insight into the potential for

DOM transformations during transit from glacial termini to coast, creates a preliminary template for gauging the current influx of P-DOM from proglacial systems to the GOA, and provides a framework that can be used to predict future DOM trends in the GOA as glaciers continue to retreat.

## 2.0. STUDY LOCATION

### 2.1. Matanuska River

This research was conducted in Southcentral Alaska (SC AK), an area which encompasses the coastline and upland regions of the central GOA, as well as the city of Anchorage and ~55% of the state's population (State of Alaska, 2020). There are more than 60 glaciers remaining in the region (Molnia, 2008), but we focused on the Matanuska Glacier (MG) and proglacial system (see Table 1 for list of location abbreviations and brief location descriptions). The MG flows north from the Chugach Mountains and terminates near the town of Glacier View, approximately 160 km northeast of Anchorage (Figure 1). The glacial outflow drains into the Matanuska River (MR), which extends from its headwaters in the Chugach Mountains to the Knik Arm near Anchorage (Curran & McTeague, 2011). The MR flows through the Matanuska Valley, between the Chugach Mountains to the south and the Talkeetna Mountains to the north, running parallel to the Glenn Highway. There are several primarily seasonal, snowmelt-fed tributaries to the MR (including Caribou Creek, Hicks Creek, Chickaloon River, and Carpenter Creek). The MG is in a transitional zone between maritime and continental climates (Kikuchi et al., 2013). The lithology of the region is varied and complex but dominated by surficial sedimentary depositions and metamorphosed sedimentary rock (Chugach flysch complex, which consists of moderately to poorly sorted sandstone, siltstone, and mudstone and metamorphosed mid-greenschist facies). The vegetation of the Matanuska Valley includes black spruce (*Picea mariana*), poplar (*Populus* spp.), white spruce (*Picea glauca*), and birch (*Betula* spp.) forests (Reed, 1956).

### 2.1. Knik/Turnagain Arm Estuary

MR discharges into the ~2,000 km<sup>2</sup> Knik/Turnagain Arm (KTA) estuary system in the upper Cook Inlet. MR merges with another proglacial river, the Knik River, immediately before draining into KTA. The Knik River contributes ~60% of the discharge, while the MR accounts for

the remaining ~40%. However, the MR is more easily accessible, which is why it was chosen as the primary study system. Other proglacial rivers that drain into the KTA estuary are Portage, Placer, and 20 Mile Rivers. The KTA estuary is subject to the sixth largest tidal extremes in the world, with a mean tidal range of 10 m (Oey et al., 2007). There are regular tidal bores with heights of up to 3 m due to the high tidal range of the Cook Inlet and the narrow, shallow configuration of the estuary arms, which amplify the tide (Molchan-Douthit, 1985). At low tide, ~500 km<sup>2</sup> of mudflats are revealed, covering approximately ¼ of the KTA estuary by area (Figure 2). They are completely exposed twice daily during actual low tide, with varying degrees of mudflat exposure during tidal transitions. These mudflats are extremely dangerous, so the KTA estuary was largely inaccessible for sampling by foot and by boat.

The KTA estuary is surrounded by >20,000 km<sup>2</sup> of wetlands (Municipality of Anchorage, 2012). Prolific wetlands are common along the GOA, yet research on wetland types, OM content and transport, and impacts on surrounding coastal systems in the region is sparse (Fellman et al., 2010a; Ford & Bedford, 1987). Fellman et al. (2010a) found that there is variation in the DOM content, composition, and bioavailability of wetlands in Southeast Alaska depending on type, highlighting the need for further analysis of diverse wetland types. Despite the lack of research regarding wetlands surrounding KTA estuary, they are an important component of the system with unquantified implications on DOM flux into the estuarine waters.

Biological activity within the KTA estuary system is limited by highly turbid waters (average = 400 – 600 Formazin Nephelometric Units; US ACE, 2017). This turbidity is caused by the influx of sediment-rich water from proglacial rivers and the strong tides, which continually resuspend deposited benthic sediment (US ACE, 2017). There is extreme vertical and lateral mixing throughout the estuary, with minimal gradients in turbidity, salinity, and even biodiversity: of the sparse marine invertebrates in the KTA estuary (<12 species identified between 1982 and 2004), most species were found in both the benthos and the water column, likely due to upheaval from vertical mixing (Houghton et al., 2005). Due to the limited penetration of sunlight throughout the estuary (Secchi disk visibility 2 – 20 cm), there is low phytoplankton biomass (Houghton et al., 2005). Diatoms can tolerate the high turbidity and survive the transition from fresh to saltwater if entering the KTA estuary via streams, so they are the dominant phytoplankton type (US ACE, 2017). Higher order animals that rely on the KTA estuary include fish (notably salmon), abundant migratory birds, and the endangered Cook Inlet beluga whales (US ACE, 2017).

### **2.3. Central Cook Inlet**

The KTA estuary connects to the Central Cook Inlet (CCI), which lies between the Kenai Peninsula to the east and Lake Clark National Park and Preserve to the west and joins the GOA to the south (Figure 1). CCI is home to a rich estuarine ecosystem that supports historic salmon and halibut fisheries. These resources were sustainably stewarded by the Dena'ina people for at least 1,000 years before colonizers forcibly relocated the original inhabitants (Boraas & Leggett, 2013; Bradner, 2015). Since then, land management has had a primarily economic rather than ecologic motivation. Today, these fisheries support the Kenaitze Indian Tribe, local recreational and subsistence fishers, and a valuable commercial fishing industry, as well as a productive and unique ecosystem.

## **3.0. METHODS**

### **3.1. Sample Collection**

The sampling sites in this study span 350 km from the Matanuska Glacier terminus (MGT), through the KTA estuary, and into CCI in the GOA (Figure 1). To characterize the nutrients and DOM fluxing from the glacier, we collected water samples from MR, the KTA estuary, and CCI, as well as from tributaries to those systems during the peak melt season from July 15-26, 2019. We sampled at the mouths of four proglacial river systems connecting to the KTA estuary for comparison with estuarine parameters (from here on referred to as riverine endmembers): Knik/Matanuska, Portage, Placer, and 20 Mile Rivers.

KTA and CCI samples were collected as close to low tide as possible, and if not possible, were collected during the outgoing tide to maximize the likelihood that riverine signatures were captured. All non-CCI samples were collected via land access. KTA estuary samples sites are numbered KTA 1 – 5 based on decreasing latitude, with KTA 1 being the northern-most site and KTA 5 being the southern-most site (Figure 1).

We collected and filtered water directly from the river and estuary using a Pegasus Alexis peristaltic pump, via sterile 0.2  $\mu\text{m}$  150 mm PTFE hydrophilic filters housed in an acrylic Geotech filtration unit, and pre-cleaned Teflon tubing. Deionized water was flushed through the tubing and filter casing prior to each sample collection, followed by 5 minutes of conditioning with the source water to remove any memory effect from the previous sample. After conditioning, the PTFE filter

was added to the casing. Samples were collected in 500 mL bottles that were pre-cleaned via nitric and hydrochloric acid baths following the protocol in Arendt et al. (2014).

CCI water samples were collected via boat along a ~100 km north-to-south transect (Figure 1) at 5 m and 30 m depths using weighted 1.5 L Teflon-coated Niskin bottles. Niskin bottles were rinsed with DI and conditioned with water at each site before collecting CCI samples. Within hours of obtaining CCI samples, they were filtered and bottled following the same protocol as the river and estuary samples. The northern-most site (CCI 1) is nearest to the KTA estuary and MR mouth, while the southern-most site (CCI 5) is nearest to the GOA (~ 150 km north of the GOA proper). Sites CCI 2 – 4 are numbered based on their relative position between CCI 1 and CCI 5 (Figure 1).

All water samples were kept cool in the field, frozen within 12 hours of collection, and shipped to home laboratories at North Carolina State University (NCSU) in Raleigh, NC for processing and analyses. At NCSU, the filtered water samples were thawed at room temperature and tested for bulk nutrient concentrations, absorbance, and fluorescence. Distance downstream of glacial terminus was determined using the “Measure Distance” tool on Google Maps.

### **3.2. *In situ* Measurements**

We used a ProDSS Handheld YSI multi-parameter meter to determine in situ pH, temperature (in °C), dissolved oxygen (DO) content (in % DO), and specific conductivity (in microsiemens  $\text{cm}^{-1}$  -  $\mu\text{S cm}^{-1}$ ) of unfiltered water for each sample collected. At the MR and KTA estuary sites, the YSI sensor was placed directly into the water and measurements taken just below the surface. CCI samples were collected at 5 m and 30 m in a Niskin, and the YSI was placed into the Niskin to measure these parameters. The YSI was calibrated daily for all parameters to ensure confidence in the measurements. One of our YSIs malfunctioned on 7/22/2019, so three samples near MGT do not have corresponding in situ data recorded for that day.

### **3.3. Bulk Nutrient Analysis**

Bulk nutrient analysis describes the concentrations of major nutrient species in water samples. It is a common method of determining longitudinal nutrient transformations, inputs, and limitations.  $C_{\text{org}}/N_{\text{org}}$  (from here-on referred to as C/N), a parameter derived from bulk nutrient analysis, is the ratio of organic C to organic N. C/N indicates nutrient limitation and DOM quality:

DOM with a low C/N is relatively enriched in N, which is a common limiting nutrient in aquatic ecosystems, and is thus considered higher quality; DOM with a high C/N has relatively little N, so it is regarded as a lower quality microbial food source (Fellman et al., 2008). DOM quality is often tied to source, so C/N can indicate DOM source material.

Concentrations of ammonia ( $\text{NH}_3$ ; detection limit =  $1.00 \times 10^4 \text{ ng L}^{-1}$ ), nitrate ( $\text{NO}_3^-$ ; detection limit =  $1.00 \times 10^4 \text{ ng L}^{-1}$ ), Total Kjeldahl Nitrogen (DON and  $\text{NH}_3$ -TKN; detection limit =  $1.00 \times 10^4 \text{ ng L}^{-1}$ ), total phosphorus (TP; detection limit =  $3.00 \times 10^4 \text{ ng L}^{-1}$ ), DOP (detection limit =  $1.00 \times 10^4 \text{ ng L}^{-1}$ ), and DOC (detection limit =  $0.10 \text{ mg L}^{-1}$ ) were determined by NCSU's Environmental and Agricultural Testing Services laboratory. Elemental concentrations were run on the Perkin Elmer 8000 Inductively coupled plasma-Optical Emission Spectrometer (ICP-OES), nutrient speciations were run on the Lachat Quikchem 8500, and DOC was run on the Shimadzu TOC/TN Analyzer. The precision rate was greater than 90 – 95%. Standards were run every 10 samples. DON was calculated as the difference between TKN and  $\text{NH}_3$ .

### 3.4. Optical Analysis

Optical analysis specifically focuses on the light-absorbing portion of DOM that can absorb incoming radiation (chromophoric DOM – CDOM). An especially useful absorbance parameter is the specific ultraviolet absorbance at a wavelength at 254 nm ( $\text{SUVA}_{254}$ ), which indicates DOM aromaticity. Fluorescent DOM (FDOM) is the portion of CDOM that absorbs and reemits light. Fluorescence spectroscopy is a useful tool for determining the source and bioreactivity of DOM, so it is regularly used in studies of glacial DOM (e.g., Barker et al., 2013; Dubnick et al., 2010; Hood et al., 2009).

DOM source, processing, and general composition are indicated by excitation/emission peaks that form at experimentally determined ranges of absorbance and fluorescence and indicate the presence of certain fluorophores (organic molecules that absorb and reemit light; Coble et al., 1998; Fellman et al., 2010b). Although the fluorescence peaks do not specifically relate to the fluorophores, they can be used to infer DOM characteristics (Fellman et al., 2010b). Peaks B and T often indicate autochthonous (from within the system), P-DOM, while peaks A, C, and M are associated with allochthonous (from outside the system), humic-like DOM (Fellman et al., 2010b). The source of peak N is unknown, but it is associated with recent, phytoplankton production (Coble et al., 1998). Further information about fluorescence peaks is summarized in Table 2. %P-DOM

was calculated as the sum of protein-like peak fluorescence over the sum of protein-like and humic-like peak fluorescence (Equation 1 in Methods). %P-DOM gives information about the bioavailability of DOM. The humification index (HIX) indicates the extent of DOM humification. Freshly produced DOM has low HIX values, while humic DOM has elevated HIX values (Huguet et al., 2009). The biological index (BIX) indicates the DOM freshness. Freshly produced, autochthonous DOM has high BIX values (>1), while more humic DOM has lower BIX values (Table 3; Huguet et al., 2009).

Although absorbance and fluorescence analysis only give information about the CDOM and FDOM portions of DOM, respectively, the outputs generally reflect the composition of the entire DOM pool (Fellman et al., 2010b). We will be referring to CDOM and FDOM as DOM for the remainder of this study.

The optical properties of DOM in the water samples were characterized in the Aquatic Biogeochemistry Laboratory at NCSU. Samples were thawed at room temperature and divided into aliquots for optical analysis. Absorbance was measured from 200-800 nm on a Varian Cary 300 UV spectrophotometer and blank corrected with Milli-Q water. Samples with absorbance of at least 0.4 at 240 nm were run in a 1 cm quartz cell, while samples with absorbance  $\leq 0.002$  at 400 nm in the 1 cm cell were run in a 10 cm cylindrical cell with quartz windows. Napierian absorption coefficients ( $a$ ) were computed using Equation 1,

$$a(\lambda) = \frac{A(\lambda_{sample} - \lambda_{blank})}{L} \times 2.303 \quad (1)$$

where  $a$  is the absorption coefficient ( $\text{m}^{-1}$ ),  $\lambda$  wavelength (nm),  $A$  is the absorbance of the sample or blank, and  $L$  is the pathlength of the quartz cell (m) (Osburn & Morris, 2003).  $\text{SUVA}_{254}$  (in  $\text{L mg C}^{-1} \text{m}^{-1}$ ) was calculated as the ratio of the decadal UV absorption at 254 nm to the DOC concentration (Barker et al., 2006; Weishaar et al., 2003).

CDOM fluorescence was measured in a 1 cm quartz cell on a Varian Eclipse fluorescence spectrophotometer, using Milli-Q water as a blank. Excitation was measured in 5 nm intervals from 240 – 450 nm, and emission was measured in 2 nm intervals from 300 – 600 nm. The resulting spectra were compiled into excitation emission matrices (EEMs). The slit widths for both excitation and emission modes were 5 nm. Corrections for the instrument's water Raman signal were applied, and the final values were standardized in quinine sulfate equivalents (ppb QSE).

%P-DOM was calculated using Equation 2,

$$\%P\text{-DOM} = \frac{\Sigma B+T}{\Sigma B+T+A+C+M} \times 100 \quad (2)$$

where B = fluorescence at peak B, T = fluorescence at peak T, A = fluorescence at peak A, C = fluorescence at peak C, and M = fluorescence at peak M. There is disagreement about the categorization of peak N as protein-like (Cheng et al., 2015; Coble et al., 1998; Kida et al., 2019), so we excluded it from Equation 2.

### 3.5. Stable Carbon Isotope Analyses

Stable carbon isotope ( $\delta^{13}\text{C}$ -DOC) analysis can be used to determine DOM source material due to variable isotopic fractionation between sources (Bianchi, 2007). Several studies have used stable and radiogenic isotopes to trace glacial DOM through trophic levels in proglacial ecosystems (Arimitsu et al., 2018; Fellman et al., 2015). Stable C isotope analysis is also commonly used in conjunction with C/N ratios to identify DOM sources to estuaries (see Figure 7 from Andrews et al., 1998).

Samples were sparged with ultrapure Argon gas for 20 minutes and analyzed on a wet chemical oxidation OI Analytical 1030D Aurora total organic carbon analyzer coupled to a Thermo Delta V Plus isotope ratio mass spectrometer (IRMS) to determine  $\delta^{13}\text{C}$ -DOC using Equation 3,

$$\delta^{13}\text{C}(\text{‰}) = \left[ \left( \frac{R_{\text{sample}}}{R_{\text{standard}}} - 1 \right) \times 1000 \right] \quad (3)$$

where  $\delta^{13}\text{C}$  is the stable isotope ratio of carbon (ppt),  $R_{\text{standard}}$  is the ratio of  $^{13}\text{C}$  to  $^{12}\text{C}$  for the known standard, and  $R_{\text{sample}}$  is ratio of  $^{13}\text{C}$  to  $^{12}\text{C}$  for the sample (Osburn & St-Jean, 2007).  $\delta^{13}\text{C}$  values were blank corrected for ultra-pure Milli-Q water and referenced to the Vienna Pee Dee Belemnite (VPDB) scale using a linear regression curve of six caffeine standards with concentrations ranging from 0.2 to 2.0 mg C L<sup>-1</sup> (IAEA-600,  $-27.7 \pm 0.04\text{‰}$ ) and two sucrose (IAEAC6,  $-10.8 \pm 0.03\text{‰}$ ) standards from the International Atomic Energy Agency (IAEA). Milli-Q blanks were run every 10 samples and precision for  $\delta^{13}\text{C}$ -DOC values was  $\pm 0.4\text{‰}$ .

### 3.6. Near-Terminus Cross-Study Data

%P-DOM and GPS coordinates were obtained from the corresponding authors of Fellman et al. (2010a) (n = 3) and Zhou et al. (2019) (n = 34) and obtained directly from Hood et al. (2009) (n = 7). %P-DOM in the aforementioned studies was calculated from the results of PARAFAC

analysis. The sum of protein-like model components is divided by the sum of all components. We excluded two points from Zhou et al. (2019) that had <0.1% glacial watershed cover and no visible source glaciers in Google Earth despite the reported distances from termini. We also excluded samples that were not directly downstream of glaciers from Hood et al. (2009) and Fellman et al. (2010a).

### 3.7. Statistical Methods

To investigate the relationships between the measured parameters and the distance from terminus or salinity, we performed a linear regression model in MATLAB R2020b. Correlations were significant for  $p$ -value < 0.05.

We compared nutrient and DOM parameters between the riverine endmembers, the KTA estuary, and CCI using a one-way analysis of variance (ANOVA) with R statistical software v4.1.0 (RStudio Team 2020). If we found evidence of statistically significant differences in the mean response variable between systems ( $P < 0.05$ ), we conducted a post-hoc Tukey HSD (honest significant difference) test to confirm differences between system pairs. We used one-way ANOVA and Tukey HSD tests to compare the distance downstream and %P-DOM of sampled locations in the comparative Himalayan, SC AK, and SE AK glacial systems.

Due to the limited nature of the dataset from the cancellation of a second field campaign from COVID-19 pandemic conditions, appropriate statistical tests for the existing dataset were limited but a data statistician was consulted to confirm all relevant tests were performed (personal communication, NCSU Data Science Consultant).

## 4.0. RESULTS

The spatial transect was divided into the following different systems based on the dynamics present along the transect: near-terminus MR (0 – 11 km from the terminus), downstream MR (>11 km from the terminus), riverine endmembers, KTA estuary, and CCI (Figure 1).

Downstream MR data were not included in our analysis because samples were collected directly downstream of tributary confluences (< 1 m downstream), before the tributary water and MR water could mix. Therefore, chemical parameters are heavily influenced by the tributaries and do not represent the impact of tributaries on the chemistry of MR. Future research should include

samples from directly upstream and further downstream of confluences to accurately gauge the significance of tributaries to the chemical composition of MR.

The majority of NH<sub>3</sub> measurements were non-detects (Tables 5, 10, 13, 15) due to the highly unstable nature of this compound, and thus we are not confident the laboratory measurements are representative of in-field compositions so we will not discuss the results further.

#### 4.1. Near-Terminus Matanuska River: 0-11 km

Environmental, DOM, and inorganic nutrient parameters were related to distance from MGT within the first 11 km downstream of the terminus.

##### *Environmental parameters*

The relationship between environmental parameters (stream temperature, alkalinity, specific conductivity, and pH) and distance from MGT with associated statistical values are included in Table 4. Within the first 11 km of the proglacial system specific conductivity ranged from 55.4 – 231.0  $\mu\text{S cm}^{-1}$  (Figure 3A), temperature ranged from 0.3 – 7.7°C (Figure 3C), from 0.28 – 0.81 mN (Figure 3B), and pH ranged from 8.15 – 9.01 (Figure 3D). Specific conductivity, temperature, and alkalinity all decreased with distance from the MGT, whereas pH increased over the same reach (Figure 3; Table 4).

##### *Bulk Nutrients*

Concentrations of major bulk nutrients are summarized in Table 5. There was no trend in DOC over the initial 11 km transect. At MGT, DOC ranged from 0.53 mg C L<sup>-1</sup> to 1.20 mg C L<sup>-1</sup> (mean = 0.89 mg C L<sup>-1</sup>). There was no discernable pattern in TKN with distance, and although NO<sub>3</sub><sup>-</sup> generally increased over the 11 km reach (from non-detects to 5.67x10<sup>4</sup> ng L<sup>-1</sup>), it was not significant (Tables 4-5; Figure 4). DON was elevated at the terminus (1.18x10<sup>5</sup> – 2.47x10<sup>5</sup> ng L<sup>-1</sup>), while the rest of the reach had much lower DON (non-detect to 7.07x10<sup>4</sup> ng). One exception is the sampling location directly downstream of the Hicks Creek confluence (see Figure 1), which was enriched in DON (3.27x10<sup>5</sup> ng L<sup>-1</sup>). There was no trend in DOP with distance, but TP decreased with distance (non-detect to 2.88x10<sup>4</sup> ng L<sup>-1</sup>; mean = 1.13x10<sup>4</sup> ng L<sup>-1</sup>; Table 5). There was no trend in C/N over the transect (n = 10). C/N at MGT ranged from 3.31 – 10.82 (Table 5).

##### *DOM*

Optical parameters are summarized in Table 6. Protein-like peaks decreased with distance (B: 0.43 – 4.35 QSE; T: 0.08 – 0.72 QSE; Figure 5A, B). Both peaks had large variability at MGT :

peak B ranged from 0.43– 4.35 QSE (mean = 2.14 QSE), while peak T ranged from 0.11– 0.72 QSE (mean = 0.28 QSE). All other peaks increased with distance (A: 0.05 – 0.57 QSE; C: 0.02 – 0.30 QSE; M: 0.03 – 0.30 QSE; N: 0.06 – 0.22 QSE; Figure 5C-F). HIX increased (0.07 – 2.75), while BIX decreased (0.42 – 1.67). BIX > 1 for two of the four tested MGT samples and two of the three tested samples from 2.22 km downstream (Figure 6).

All humic-like peaks (Figure 5C-E) increased notably after the confluence with Hicks Creek (Table 9). Peaks B, T, and N and BIX had moderate increases downstream of the confluence (Figure 5A, B, F; Figure 6B). %P-DOM decreased over the 11 km transect (50.37 – 96.54%; Table 7; Figure 7).

The  $\delta^{13}\text{C}$ -DOC content of three MGT samples ranged from -22.60 to -31.22‰ (mean = -27.31‰). Averages are displayed with accompanying C/N in Table 8. Potential DOM source material is displayed in a biplot of  $\delta^{13}\text{C}$ -DOC and C/N (Figure 8).  $\delta^{13}\text{C}$ -DOC and SUVA<sub>254</sub> are plotted in Figure 9.

#### *Tributary Influence: 0-11 km*

Non-glacial Hicks Creek is primarily snowmelt-driven and intersects MR at 10.69 km downstream. Hicks Creek was elevated in DOC and all fluorescence peaks relative to the average of the samples directly upstream of the confluence (Table 9).

## **4.2. Knik-Turnagain Arm (KTA) Estuary**

### *Bulk Nutrient*

Estuarine bulk nutrients for each salinity are compiled in Table 10, and associated statistical values are in Table 11.

One C/N value (C/N = 140) was identified as an outlier (greater than 1.5 times the quartile range, Grubb's test  $P < 0.0001$ ), so it was excluded from analysis. We excluded DOC and DON for that sample as well for consistency. C/N ratios decreased with increasing salinity (4.53 – 23.07; mean = 10.82; Figure 10C). This was largely driven by primarily driven by decrease in DON ( $9.04 \times 10^4$  –  $2.84 \times 10^5$  ng L<sup>-1</sup>; Figure 10B). DOC did not vary significantly with distance (mean = 1.30 mg L<sup>-1</sup>; Figure 10A).

### *DOM*

Estuarine optical parameters for each salinity are compiled in Table 12, and associated statistical values are in Table 11.

Peaks N, C, and M all decreased as salinity increased (N: 0.23 – 0.78 QSE; C: 0.24 – 1.02 QSE; M: 0.22 – 1.03 QSE; Figure 10D-F). There were no trends with salinity in peaks A, B, or T (A: 0.49 – 2.17 QSE; B: 0.54 – 1.66 QSE; T: 0.26 – 0.49 QSE). Both BIX and HIX decreased as salinity increased (BIX: 0.46 – 0.83 QSE; HIX: 0.76 – 7.03 QSE; Figure 10G-H).

There was no trend in % P-DOM with salinity (23.70 – 46.62%; mean = 33.59%), but the low values relative to proglacial rivers indicate that the FDOM is largely humic-like. SUVA<sub>254</sub> did not have a significant trend but tended to decrease as salinity increased (0.67 – 3.50 L mg C<sup>-1</sup> m<sup>-1</sup>; Figure 10I).  $\delta^{13}\text{C}$ -DOC was measured for all KTA samples and values ranged from -26.77‰ to -30.65‰ (mean = -28.70‰; Table 8).

### 4.3. Riverine Endmembers

We collected a total of 9 samples from the riverine endmembers: Knik/Matanuska (n = 3), Portage (n = 2), Placer (n = 2), and 20 Mile Rivers (n = 2). Major bulk nutrients for the riverine endmembers are listed in Table 13, and optical properties are listed in Table 14. DOM was consistently proteinaceous (45.70% - 70.47% P-DOM; mean = 60.74%). The average NO<sub>3</sub><sup>-</sup> was 2.90x10<sup>4</sup> ng L<sup>-1</sup> (two values below the detection limit; max = 6.77x10<sup>4</sup> ng L<sup>-1</sup>), and the average DON was 8.20x10<sup>4</sup> ng L<sup>-1</sup> (three values below the detection limit; max = 2.90x10<sup>5</sup> ng L<sup>-1</sup>).

We calculated the approximate hourly discharge of DOC from the Matanuska/Knik River into the KTA estuary by dividing the average DOC of that site by the hourly discharge from gage data for the Matanuska and Knik Rivers <20 km upstream of their confluence with the KTA estuary for our sample collection time. We determined that the Matanuska/Knik River was exporting an average of ~3,000 kg DOC hr<sup>-1</sup> during our sampling campaign.

### 4.4. Central Cook Inlet (CCI)

There were no significant trends in major bulk nutrient, fluorescence, or environmental parameters with distance along the CCI transect (n = 20 for all measurements). Salinity increased between 5 m and 30 m depths (n = 10 per depth; *P* < 0.01), but all other major parameters, including fluorescent peaks and indices, DOC, and nitrogen species, had no significant differences. Major nutrient concentrations and optical properties for CCI are listed in Table 15 and Table 16, respectively.

There was no trend in  $\delta^{13}\text{C}$ -DOC with distance along the transect or with salinity (mean =  $-27.28\text{‰}$ ; Table 8). The combined  $\delta^{13}\text{C}$ -DOC and C/N values corresponded to freshwater algae as the source material at CCI 1, marine algae at CCI 2 and CCI 4, and C3 terrestrial plant at CCI 3 and 5 (Figure 8).

#### 4.5. Differences between Systems

We investigated statistical differences between the chemical compositions of samples from the KTA estuary and its riverine and CCI endmembers. The KTA estuary had significantly greater means than the riverine endmembers for  $\text{NO}_3^-$ , DOC, peaks A, C, M, and N, HIX, and  $\text{SUVA}_{254}$  (Table 17; Figures 11-16).

The riverine endmembers had significantly greater mean %P-DOM than the KTA estuary (ANOVA: F-value = 25.9,  $P = 1.72 \times 10^{-7}$ ), with a difference of 27.13% P-DOM (Figure 17). The KTA estuary had significantly elevated means relative to CCI in the following notable parameters:  $\text{SUVA}_{254}$  and peaks A, C, and M (Table 18; Figures 13, 16).

Although the difference between DOC in the KTA estuary and CCI was not statistically significant ( $P = 0.06$ ), the range of non-outlier CCI samples ( $1.11 - 2.04 \text{ mg L}^{-1}$ ) encapsulated an elevated DOC range compared to the range of non-outlier DOC values from the KTA estuary ( $1.07 - 1.40 \text{ mg L}^{-1}$ ; Figure 12).

#### 4.6. Near-Terminus Cross-Study Comparison

We analyzed samples collected in the Himalayas (from Zhou et al. 2019), SC AK (from Hood et al. (2010) and original data from this study), and SE AK (from Hood et al. (2009), Fellman et al. (2010a; Table 19). All samples were collected within  $\sim 25$  km downstream of termini (Himalayas: 0.0 – 26.6 km; SC AK: 0.0 – 22.0 km; SE AK: 6.9 – 12.1 km). There was not a significant difference in the mean distances from terminus in each region ( $P = 0.84$ ). However, mean %P-DOM differed between all three systems (Himalayas: mean = 81.3%; SC AK: mean = 66.0%, SE AK: mean = 31.1%;  $P = 2.64 \times 10^{-7}$ ). Tukey HSD tests revealed significant differences in the mean %P-DOM between SC AK and the Himalayas ( $P = 6.88 \times 10^{-3}$ ), SE AK and the Himalayas ( $P = 3.00 \times 10^{-7}$ ), and SE AK and SC AK ( $P = 4.01 \times 10^{-4}$ ). %P-DOM decreased with distance in all locations, although with varying rates (Figure 18; Table 20).

## 5.0. DISCUSSION

### 5.1. %Protein-like DOM from Terminus to 11 km

Over the first 11 km of the Matanuska River P-DOM was released from MGT and preferentially consumed in transit. We observed high %P-DOM near the terminus (within ~2 km from MGT; mean = 88.37%; n=7) that significantly decreased over this distance. The combined  $\delta^{13}\text{C}$ -DOC and C/N suggested bacterial origins, and indicators of recent microbial production, such as peaks B and T and BIX, were elevated near the terminus (Figures 5A-B, and 6B). These parameters strongly suggests that terminus DOM is microbial in origin (Fellman, et al., 2010). These findings corroborate studies in Alaska, the Alps, the Himalayas, Greenland, and Antarctica that identified protein-rich DOM from supraglacial algae and cryoconite holes and subglacial microbial populations in near-terminus proglacial streams studies (Barker et al., 2013; Bhatia et al., 2010; Singer et al., 2012; Stubbins et al., 2012; Zhou et al., 2019).

We suspect that the variability in protein-like peaks and BIX at MGT is due to changes in factors influencing the proportion of supra- vs. subglacial melt in runoff between sampling dates (Hodson et al., 2008; Hotaling et al., 2017). For example, warmer air temperature on a sampling date might elevate supraglacial melting and hydrologic connectivity between the sub- and supraglacial environments, increasing the amount and rate of supraglacial discharge delivery to subglacial and proglacial systems (Hodson et al., 2008; Hotaling et al., 2017). Supraglacial DOM is derived from cryoconite holes, which have biodiverse microbial communities, and surface algae, both of which are spatially heterogenous across the surface (Hodson et al., 2008). Despite variations in supraglacial runoff, it tends to contain higher and less variable %P-DOM than subglacial runoff (Bhatia et al., 2010).

Subglacial DOM dynamics are complex because they depend on hydrologic connectivity and inputs from overridden soil in addition to *in situ* production (Bhatia et al., 2010). When the sub-, supra-, and proglacial environments are hydrologically connected (usually corresponding to periods of high runoff), supraglacial inputs are elevated, and water moves quickly into proglacial streams (Bhatia et al., 2010; Hotaling et al., 2017). Our sampling campaign occurred during peak melt during periods of high runoff for the Matanuska Glacier system. Although the subglacial signature during periods of elevated runoff largely resembles that of supraglacial DOM, the influx of supraglacial water can flush terrestrial DOM in overlain subglacial soils into the proglacial

system, adding a stronger humic signature to the runoff that we did not observe in our study (Barker et al., 2009; Bhatia et al., 2010). When hydrologic connectivity is still developing early in the melt season in the subglacial system, connectivity is limited, and pockets of water can exist in isolation with limited external inputs. This allows for longer residence times of water in the subglacial system, which extends water-rock interaction times and allows for bacterial processes to alter subglacial DOM until later in the melt season when there is enough connectivity to drain the water (Barker et al., 2009; Hodson et al., 2008). The proportion of supraglacial and subglacial inputs to the proglacial systems can vary on daily, in addition to seasonal, timescales (Arendt et al., 2015). The variability observed at MGT is likely due to changing proportions from the sub- and supra-glacial systems, emphasizing the importance of repeat measurement at the terminus to capture a longer-term average.

#### *Protein-loss Mechanisms*

We believe that microbial degradation is the likely explanation for the decrease in %P-DOM in our system. There was evidence of both humic-like DOM additions and protein-like DOM losses over the 11 km transect, both of which would decrease %P-DOM. Despite the DOM additions, bulk DOC decreased over the transect, indicating that DOM losses exceed additions. Downstream of the terminus BIX and peaks B (tyrosine-like) and T (tryptophan-like) decreased significantly with distance (Figures 5A-B, 6B). Incubation studies have demonstrated that tyrosine-like and tryptophan-like glacial DOM is highly bioavailable and subject to microbial consumption (Fellman et al., 2015; Hood et al., 2009; Singer et al., 2012; Zhou et al., 2019). These studies and our own findings indicate selective removal of protein-like DOM downstream of MGT, in which microbes preferentially consume proteinaceous material due to its highly labile nature.

We also saw a significant increase in  $\text{NO}_3^-$  over the initial 11 km (Figure 4). This might be due to the microbial conversion of DON to DIN via ammonification (DON is converted into  $\text{NH}_3$ ) and nitrification ( $\text{NH}_3$  is converted into  $\text{NO}_3^-$ ), as was observed in glaciers in the Alps (Singer et al., 2012). However, there was no corresponding change in DON, so it is unclear if the trend in  $\text{NO}_3^-$  is due to microbial DOM degradation.

Photodegradation is a common pathway for DOM transformation in non-glacial streams (Brooks et al., 2007). DOM is photoreactive, and thus susceptible to loss and alteration of absorption and fluorescence properties (Bianchi, 2007). In Arctic Alaskan rivers, extended summer daylight allows for elevated photodegradation (Cory et al., 2007). Extended daylight

during peak melt season in SC AK might similarly enhance photodegradation in MR. Further research on photodegradation in proglacial rivers is warranted to investigate potential impacts on DOM composition and bioavailability.

#### *Sources of humic-like DOM*

Downstream of MGT, humic-rich DOM was added to MR. Between MGT and the Hicks Creek confluence, the humic-like peaks (A, C, and M) increased (Figure 5C-E). We suggest two possible sources of this additional humic-rich DOM: 1) microbial degradation of P-DOM, which can increase humic substances (Guillemette & Giorgio, 2012; Yamashita et al., 2011) and 2) OM inputs from soil – which is rich in humic DOM – as MR flows through increasingly mature soils, as was seen in southeastern Alaska and the Himalayas (Hood et al., 2009; Zhou et al., 2019). Directly downstream of Hicks Creek (10.72 km from MGT), there is a steep spike in all three humic-like peaks (Figure 5). This corresponds to the addition of Hicks Creek's humic-rich discharge, indicating the importance of lateral DOM inputs from non-glacial tributaries. Several other studies have similarly found that non-glacial tributaries are significant sources of humic-like DOM to proglacial rivers (Barker et al., 2009; Zhou et al., 2019).

#### *Implications*

This pilot study is the first to capture longitudinal changes in proglacial stream DOM in Alaska. The GOA ecosystem is strongly influenced by its proglacial tributaries, which carry massive amounts of freshwater, sediment, and labile DOM from glacial termini (Hood et al., 2009). It is essential to investigate the degree to which glacially-sourced labile P-DOM is consumed before delivery to marine waters. Otherwise, scientists risk overstating the impact of glacial DOM contributions to coastal systems when the glacial signature is lost before reaching the coast. Defining a distance threshold of glacially sourced DOM will allow scientists and resource managers to better understand and predict impacts on downstream ecosystems with climate change and inevitable glacial recessions. Our proglacial findings indicate that P-DOM from the Matanuska Glacier is rapidly and selectively consumed, most likely via microbial pathways. Within the first 11 km of MR, %P-DOM decreases an average of ~25%, or approximately  $2.5\% \text{ km}^{-1}$ . Presumably, the remaining bioavailable proteinaceous matter continues to be microbially reworked as it is transported further downstream and ultimately depleted, as was seen in Himalayan proglacial streams (Zhou et al., 2019).

The vast majority of glaciers along the GOA are retreating in response to climate change (Arendt et al., 2002). The relationship between %P-DOM and distance from terminus in MR can provide a template for estimating changes in the delivery of P-DOM to the GOA as the length of proglacial rivers increase with glacial retreat. For example, Bear Glacier, which feeds into the GOA on the southeast side of the Kenai Peninsula, was recently a tidewater glacier that has since retreated from the coast, creating a new proglacial environment between the terminus and the ocean. Bear Glacier's rate of retreat has substantially increased in recent years and will likely continue to do so as the climate warms (Kurtz, 2019). From 2000 – 2019, Bear Glacier retreated approximately 5.3 km, which we estimate corresponds to a ~13.5% reduction in %P-DOM it delivers to the coast. Proglacial streams are lengthening throughout the region with inevitable changes to associated DOM fluxes. These changes in proglacial reach length have poorly constrained and potentially severe consequences for downstream marine ecosystems that should be prioritized in future research efforts. Organisms throughout the GOA food web (including various species of plankton, invertebrates, fish, and seabirds) rely on the annual flux of protein-rich DOM from glaciers (Arimitsu et al., 2018; Fellman et al., 2015). The GOA ecosystem will be forced to adapt as this source of readily bioavailable nutrients diminishes with accelerating climate change.

The implications of the loss of labile DOM as it is delivered from glacial terminus to the GOA via proglacial rivers have not been previously considered or accounted for in regional or global models. Our findings provide a preliminary template for constraining previous estimates of labile glacial DOM delivery to the GOA. For example, Hood et al. (2009) estimated that  $0.13 \pm 0.01 \text{ Tg C yr}^{-1}$  is delivered to the GOA by proglacial streams, of which ~66% (~0.1 Tg C yr<sup>-1</sup>) was suggested to be highly bioavailable (high %BDOC). The Hood et al. (2009) % BDOC estimate is derived from the finding that ~66% of the riverine DOC in the highly glaciated Sheridan River in SC AK near Valdez was readily degraded by marine microbes and DOM consisted of 77% P-DOM. However, it is important to note that the Sheridan River sample site was ~5.5 km downstream of Sheridan Glacier and ~15 km from the GOA. We can update Hood et al.'s estimate of %BDOC delivered to the GOA by accounting for %P-DOM losses over the remaining 15 km to the ocean. If P-DOM in the Sheridan River is degraded at the same rate as in MR and the relationship between %P-DOM and % BDOC found in Hood et al. (2009) remains consistent, only ~50% (rather than the originally estimated 66%) of the DOM delivered to the GOA in the Sheridan

River will be highly bioavailable. When this revised estimate is scaled to the entire influx of glacial runoff to the GOA as done in Hood et al. (2009), approximately  $0.065 \text{ Tg C yr}^{-1}$  of labile DOC is delivered in glacial runoff. The decrease in %P-DOM with distance from terminus must be accounted for in climate models to accurately represent the role of glaciers in the global carbon cycle.

## 5.2. Near-Terminus Cross-Study Comparison

We placed our proglacial data into a larger context using comparisons with previously published DOM data from Alaskan (Fellman et al., 2010a; Hood et al., 2009) and Himalayan (Zhou et al., 2019) proglacial streams. In line with our study approach, these papers used fluorescence spectroscopy to examine their proglacial data. Rather than using fluorophore peaks to analyze excitation-emission data, however, these studies used parallel factor (PARAFAC) analysis. PARAFAC decomposes DOM fluorescence into separate components and estimates the relative contribution of each component to the total fluorescence (Fellman et al., 2010b). %P-DOM is calculated by dividing the protein-like components (similar but not identical to the protein-like peaks B and T) by the sum of the components. Although the %P-DOM values are likely similar between methods, these different approaches to investigating %P-DOM do not allow for direct comparisons between our numerical outcomes. However, the trends observed with %P-DOM and distance are in agreement and provide a greater understanding between the relationship of these parameters in different glacial environments.

Zhou et al. (2019) investigated DOM properties and transformations in a wide range of Himalayan proglacial streams and rivers ( $n$  for proglacial samples = 77). Although the climate regime and continental location of these study locations differ from southcentral AK, similar relationships between distance from terminus and %P-DOM are observed. The Himalayan streams are located in the northern Tibetan Plateau and the Gobi Desert, where the climate is arid and extremely cold (Zhou et al., 2019). Similar to the trends observed from our original data, Zhou et al. (2019) found that P-DOM was enriched near glacial termini and decreased significantly with increasing distance from terminus. Incubation experiments with proglacial inoculum confirmed that selective microbial removal of P-DOM was responsible for the observed trends in P-DOM (Zhou et al., 2019). Zhou et al. (2019) also implicated non-glacial tributaries as sources of humic-

like DOM downstream of the termini. We included 32 proglacial samples from Zhou et al. (2019), all collected within 30 km of various glacial termini in our comparative analysis.

Studies by Hood et al. (2009) and Fellman et al. (2010a) examined the relationships between glaciated watershed cover, % BDOC, and %P-DOM in Alaska (Hood: SE and SC AK; Fellman: SE AK). These study locations are similar to the coastal environment investigated in our original study. However, the proglacial streams from Hood et al. (2009) and Fellman et al. (2010a) all terminated within ~20 km of the coast. We used data from the Hood et al. (2009) and Fellman et al. (2010a) streams that receive direct glacial runoff (Hood:  $n = 7$ ; Fellman:  $n = 3$ ). In SE AK, both studies sampled from the same location in Lemon Creek and Mendenhall Rivers, and Fellman et al. (2010a) also sampled Eagle/Herbert River. In SC AK, Hood et al. analyzed samples from Sheridan and Scott Rivers near Cordova, AK and Portage, Placer, and 20 Mile Rivers near Anchorage, which feed into the KTA estuary. We also sampled Portage, Placer, and 20 Mile Rivers (roughly identical to Hood's sites for Placer and 20 Mile, ~10 km downstream of Hood's site for Portage). Hood et al. (2009) and Fellman et al. (2010a) sampled the proglacial rivers at approximately peak melt, which is when we collected samples in SC AK (Fellman: June; Hood: late July; our study: mid-late July), so seasonal influences between studies should be similar.

The majority of sample locations from SC and SE AK have similar and overlapping climates. SE AK and the eastern portion of SC AK (which includes Sheridan, Scott, Placer, Portage and 20 Mile Rivers) are in a maritime climate that is characterized by a maritime climate and temperate rainforest biome (Hood et al., 2009). However, the northwest portion of SC AK, where the Matanuska Glacier is located, is in a transitional maritime-continental climate zone that experiences more seasonal temperature variability and less precipitation (Kikuchi et al., 2013).

The combined data from these three studies (Hood et al., 2009; Fellman et al., 2010a; Zhou et al., 2019) and our original data provides a first comparative look into %P-DOM variation with distance between different proglacial streams: the Himalayas, SE AK, and SC AK (Figure 18). Zhou et al. (2019) provides a robust and comprehensive characterization of Himalayan proglacial streams. Because Himalayan geography and climate are unique from our original SC AK site, the climatic and environmental influences on these differing systems are not comparable and the data from these locations were analyzed separately. While we cannot directly compare our SC AK %P-DOM values to those from Hood et al., (2009) due to our different %P-DOM approaches, we

grouped our original data with theirs to show the general range of values and trend for the SC AK region (combined Hood et al. (2009) SC AK data and near-terminus original data  $n = 21$ ).

All three glacial regions (Himalayas, SE AK, and SC AK) showed decreasing % P-DOM with distance, confirming our findings for the Matanuska River (Fig #). In the Himalayas, DOM near the glacial terminus (within 2 km) averaged  $91.4\% \pm 2.22\%$  protein-like ( $n = 9$ ). This is similar to the average % P-DOM within 2 km of MGT in SC AK (mean =  $88.40\%$ ,  $n=7$ ). Downstream of the termini, however, regional patterns begin to emerge (Figure 18).

The mean %P-DOM values of the three glacial regions were significantly different ( $P = 2.64 \times 10^{-7}$ ). The Himalayas had the highest average %P-DOM ( $81.3\%$ ), followed by SC AK ( $66.0\%$ ), then SE AK ( $31.1\%$ ). Although the three regions had samples from different ranges of distances, there was no significant difference in the average distance downstream of terminus for the three data sets. Therefore, the disparities in mean %P-DOM between the three regions might reflect environmental differences between the glacial systems.

Without additional data from SE AK and directly comparable data from SC AK (%P-DOM data obtained via same methodologies) we cannot speculate about differences in %P-DOM between the two Alaskan subregions. Our analysis of the SC AK samples from Hood et al. (2009) suggested a slight relationship between %P-DOM and distance from terminus, although it was not significant ( $R^2 = 0.59$ ;  $P = 0.13$ ;  $n = 5$ ; Table 20). Our analysis of combined SE AK samples from Hood et al. (2009) and Fellman et al. (2010a) showed a strong relationship between %P-DOM and distance from terminus ( $R^2 = 0.88$ ;  $P = 0.02$ ;  $n = 5$ ; Figure 18; Table 20). Future efforts to compile %P-DOM data from proglacial streams during peak melt season in the two subregions are warranted. Additionally, time-series datasets would provide further insight to the temporal variability of DOM characterization and should be a goal of future studies.

There is a clear difference in %P-DOM between the Himalayan and Alaskan systems. At the terminus, %P-DOM in the Himalayas and SC AK are very similar. Downstream, however, SC AK %P-DOM decreases at a quicker rate than Himalayan %P-DOM. Zhou et al. (2019) attributed discrepancies in their %P-DOM and Hood et al.'s (2009) reported %P-DOM to the extreme difference in climate between the Himalayas and Alaska. In the dry, high-altitude Himalayas, the limited rainfall and vegetation minimize humic inputs from surrounding terrestrial ecosystems (Zhou et al., 2019). Coastal Alaska has lush temperate rainforests, OM-rich soils, and significant precipitation that export substantial humic-rich DOM to proglacial streams as they travel through

downstream ecosystems (Fellman et al., 2014). These extra humic inputs might be responsible for the accelerated rate of %P-DOM decline in Alaskan proglacial streams.

Another possibility is that variations in physicochemical factors between regions determine the rate at which microbes respire P-DOM in proglacial streams. This might be a direct control: temperature can inhibit rates of microbial respiration (Manning et al., 2018), and the high-elevation Himalayan mountains tend to be cooler than the low-elevation, marine-influenced Alaskan coast. Alternately, physicochemical factors in each region might favor different microbial community structures that respire DOM at disparate rates. Wilhelm et al. (2013) found that microbial community structure in proglacial streams in the Alps is controlled by pH, temp, and conductivity. These findings were confirmed in Himalayan proglacial streams, where Ren et al. (2017) found strong relationships between microbial diversity and community composition and pH, temperature, and distance downstream of terminus. The authors proposed that proglacial stream microbes have “...specialized physiological and functional adaptations to the particular hydrological and physicochemical environments of these harsh systems...” and suggested that gradients in stream physicochemical conditions might explain shifts in microbial community structure along the reach of proglacial streams (Ren et al., 2017). Our own data validate that physicochemical gradients exist in proglacial streams: pH, temperature, specific conductivity, and alkalinity in MR were very strongly correlated with distance downstream of MGT (Figure 3). These studies indicate that climatic (impacts stream temperature) and lithological (impacts pH and specific conductivity) differences might explain the disparity in the rate of % P-DOM decrease between Himalayan and SC Alaskan proglacial streams.

Our preliminary compilation of %P-DOM in diverse glacial environments indicates that the selective removal of proteinaceous material immediately downstream of glacial termini is a common phenomenon and hints at region-specific influences on the rate of removal. As glaciers retreat globally and proglacial streams increase in length, understanding the regional rates of %P-DOM decrease will help predict downstream ecosystem impacts. This is especially crucial in coastal systems such as SC AK and SE AK, where glacial water chemistry has profound implications for downstream marine ecosystems. Future work should supplement the compiled Alaska data, incorporate proglacial %P-DOM from other regions such as Antarctica and Greenland, and explore the connections between physicochemical stream-water characteristics and microbial functioning in proglacial streams.

### 5.3. KTA Estuarine DOM Dynamics

We were forced to cancel our second field season in response to the COVID-19 pandemic and found our intended pilot dataset was insufficient by itself to determine if we could track DOM from MGT to the GOA. However, our pilot study results indicate that there are multiple notable sources of DOM to the coastal system in addition to MR. During our initial field campaign, we sampled at the mouths of four (Matanuska/Knik, Portage, Placer, and 20 Mile Rivers) of the seven proglacial river systems that drain into the KTA estuary system (sample collection from other rivers limited by accessibility). Based on our analyses, these four river systems were contributing substantial runoff and DOC to the KTA estuary: the Matanuska/Knik River alone was exporting approximately 3,000 kg DOC hr<sup>-1</sup> during our sampling period, of which ~65% was protein-like and likely labile. Without higher spatial resolution in our sampling, however, we could not trace that DOC through the estuary. Instead, we compared the nutrient characteristics of the riverine endmembers to those within the KTA estuary to speculate about allochthonous DOM sources and *in situ* microbial metabolism.

We did not sample the KTA estuary longitudinally, so salinity is not a suitable proxy for distance from the mouth of MR. Differences in salinity between our samples are caused by the balance of river discharge and tidal variations, both of which are defining characteristics of the KTA estuary. Tides have been observed to contribute marine DOM to estuaries (Fellman et al., 2011; Yamashita et al., 2011). The high tidal ranges in both arms of the estuary mean that there is a temporal dynamism in the system: the biogeochemical parameters of the estuary are partially dependent on the state of the tide at a given time. Sample collection in the KTA estuary targeted low tide to maximize the influence of proglacial rivers, hence the low salinities of our samples. In this system, currents can reverse from an ebb tidal velocity of 6 m s<sup>-1</sup> to a flood velocity of 10 m s<sup>-1</sup> over the course of a few minutes, and the water level can rise up to 10 cm min<sup>-1</sup> (Deboer, 2009). Our salinity range likely reflects the distribution of sampling times around low tide and the velocity of the outgoing and incoming tides on different collection days. This can be seen in samples collected ~200 m apart within 10 – 20 minutes of each other that have a range of salinities (Tables 10, 12).

#### *Allochthonous DOM sources*

We found that the mean DOC in the KTA estuary was more than double that of the riverine endmembers (Figure 12). Although both humic-like and protein-like fluorescence increased

between the riverine endmembers and the KTA estuary, the rise in humic-like DOM was much more pronounced. Measures of DOM quality such as %P-DOM (Figure 17) and SUVA<sub>254</sub> (Figure 16) indicated that DOM in the estuary was more aromatic and less labile than that in the riverine endmembers. This influx of recalcitrant, humic-like material to the KTA estuary points toward allochthonous, terrestrial DOM sources.

One probable source of allochthonous DOM is the >20,000 km<sup>2</sup> of surrounding wetlands, many of which are intertidal (Figure 1; Municipality of Anchorage, 2012). Coastal wetlands can export abundant DOC to nearby marine systems (Alkhatib et al., 2007; Baum et al., 2007; Fellman et al., 2008). We speculated that the incoming tide suspends the intertidal wetland OM, and the outgoing tide transports it to the estuary, as was suggested in Houghton et al.'s (2005) summary of Knik Arm ecology. We also suspect that nearby supratidal wetlands contribute DOM through surface and groundwater contributions (Cawley et al., 2014).

To determine if the surrounding wetlands are a potential source of DOM to the KTA estuary, we compared the optical properties of our least saline sample from the KTA estuary to those of soil OM in southeastern Alaskan wetlands near the GOA (Fellman et al., 2008). The SUVA<sub>254</sub> of our sample (3.29 L mg C<sup>-1</sup> m<sup>-1</sup>) was comparable to that of fens (a type of peat-forming wetland common at mid-high latitudes) in SE AK (3.51 L mg C<sup>-1</sup> m<sup>-1</sup>), indicating comparable aromatic C contents (Fellman et al., 2008). Our KTA estuary %P-DOM (29.71%) was similar to that of the southeastern AK fens (23.4%). The other wetland types sampled in Fellman et al. (2008) had more elevated SUVA<sub>254</sub> and lower %P-DOM than our system. If wetlands surrounding the KTA estuary resembled those more humic wetland types, the dilution of wetland runoff with the fresher proteinaceous proglacial river runoff might explain the disparity in DOM quality.

We also compared  $\delta^{13}\text{C}$ -DOC at the least saline KTA estuary site (-28.88‰) to  $\delta^{13}\text{C}$ -DOC in North American coastal wetlands. Major deviations might indicate that wetlands are not a notable source of DOM to the KTA estuary. Our value was within the -25.2 to -29.4‰ range of North American coastal wetlands, so wetlands cannot be dismissed as a potential DOM source (Opsahl, 2005; Raymond & Bauer, 2001; Rudolph et al., 2020) but additional investigations are needed to characterize the KTA wetland-derived DOM.  $\delta^{13}\text{C}$ -DOC and SUVA<sub>254</sub> values of the least saline KTA estuary sample were comparable to that of wetlands in the coastal plains of the southern United States (Figure 9). Additionally, the near-shore Peterson Creek in SE AK (potentially similar to those transporting wetland DOM to the GOA in SC AK) has a heavy wetland

presence and averaged a comparable  $\delta^{13}\text{C}$ -DOC value of  $-28.4 \pm 0.1\%$ , indicating that wetland streams might be delivering DOM to the KTA estuary (Fellman et al., 2015). Our preliminary comparison between allochthonous DOM in the KTA estuary and wetland DOM in SE AK and other published studies with similar DOM data supports our theory that nearby and intertidal wetlands are potential sources of estuarine allochthonous DOM in the KTA estuary.

Another likely source of allochthonous DOM to the KTA estuary is the extensive mudflats ( $>500 \text{ km}^2$ ) that are exposed at low tide (Figure 2). Although we did not sample directly from the mudflats, previous studies have found that mudflats, including similarly sized intertidal mudflats in the proglacial Copper River Delta in SC AK, are regions of high primary productivity and abundant infaunal benthic invertebrates (Dube, 2012; Powers et al., 2002). In the Copper River Delta, riverine and marine OM was deposited on the sediments, consumed by benthic algae, and transferred up the estuarine food web (Powers et al., 2005). The KTA estuary is subject to extreme vertical mixing, in which benthic sediments, organisms, and OM accumulated on mudflats during low tides are regularly resuspended and remixed by the strong tides in the region (US ACE, 2017; Mulherin et al., 2001). Based on this, resuspended DOM from the mudflats is a likely source of allochthonous DOM in the estuary. Without samples from the mudflats, however, we cannot verify their contribution to estuarine DOM. Future research should investigate the role of mudflats in KTA estuary biogeochemical processing.

At higher salinities, the marine influence on estuarine DOM composition was apparent. Although CCI had more elevated DOC than the KTA estuary throughout, it had significantly lower mean peak intensities for all fluorescence peaks except peak T. CCI also had relatively high C/N ratios (mean = 23.22), which generally signals that the DOM is lower quality (Alkhatib et al., 2013). When C/N was related to  $\delta^{13}\text{C}$ -DOC, vascular C3 plants (typically more recalcitrant than planktonic-derived OM) were identified as the primary DOM source (Figure 8). This indicates that the dominant DOM signature in CCI is from terrestrial inputs, rather than the more proteinaceous glacial or autochthonous inputs. The KTA estuary progressively resembled CCI's DOM profile as salinity increased: DOC and C:N ratios increased, peak M, C, and N fluorescence decreased, and the DOM skewed toward a C3 plant signature. These findings suggest that the CCI DOM signature progressively overrides that of other DOM sources as the tide rises.

#### *Autochthonous DOM Production*

Although our KTA estuary samples were dominated by allochthonous DOM signatures, we found evidence of internal microbial production as well. While the riverine endmembers had low levels of  $\text{NO}_3^-$  (Table 13),  $\text{NO}_3^-$  levels dramatically increased in the KTA estuary. DON increased as well, but by a smaller margin than most other parameters. We suspect that this pattern is caused by the microbial respiration of DOM, which converts DON to  $\text{NO}_3^-$  via ammonification and nitrification. The modest increase in DON relative to DOC and other nutrients implies that some DON was added to the estuary but converted into  $\text{NO}_3^-$  via respiration. The substantial increases in peaks N and T, which both signify recent autochthonous production, is evidence that respiration contributed to microbial biomass and subsequent internal DOM production. Our results suggest that DOM inputs to the KTA estuary are sustaining microbial respiration and biomass.

Given the samples and data we have, we cannot quantitatively determine the source of the DOM used by estuarine microbes, but it is likely that the relatively P-DOM from proglacial rivers is contributing to some degree. These results highlight the ecological importance of labile DOM inputs to the KTA estuary. As inputs to the KTA estuary rapidly change, it is unclear how and at what rate this food web will adapt.

## 6.0. CONCLUSIONS

Proglacial rivers and estuaries in the GOA are complex, dynamic systems that control the flux of DOM from land-terminating glaciers to the ocean. This study was the first longitudinal characterization of DOM alterations in a transitional (glacial-fluvial-estuarine-coastal) proglacial system in Alaska. Our findings are two-fold:

First, DOM at MGT was highly proteinaceous. Almost immediately upon release into the proglacial river, %P-DOM decreased with distance over the first 11 km of MR. The decrease of %P-DOM resulted from both selective, likely microbial removal of highly labile P-DOM and lateral influx of humic-like DOM from tributary systems. Our comparison with Hood et al. (2009), Fellman et al. (2010a), and Zhou et al. (2019) yielded a first look at regional differences in the removal rate of P-DOM in pro-glacial rivers. This juxtaposition suggested that regional environmental factors are important in determining rate of P-DOM removal in proglacial streams. Second, the DOM signature within the estuary differed greatly from that of the proglacial riverine endmembers, signaling that non-glacial DOM sources and internal metabolic processes influence the KTA estuary's DOM composition more than glacially-derived DOM. The presence of adjacent

ecosystems and the chemical composition of the estuarine DOM suggest that wetlands, intertidal mudflats, the tidal influx of CCI water, and internal respiration of DOM are likely additional non-glacial sources of DOM to the KTA estuary. Our findings highlight the importance of estuaries as intermediaries between terrestrial systems, such as inland glaciers and nearby wetlands, and coastal systems in the GOA. We cannot predict how progressive glacial melt and retreat will influence the GOA without accounting for estuarine DOM sources and processes.

The dramatic transformation of the cryosphere with climate change carries global repercussions for downstream ecosystems (Huss & Hock, 2018; Milner et al., 2017). Because glaciers deliver abundant fresh water, DOM, and sediments downstream, it is critical to understand how their retreat will affect the biological and anthropogenic systems that rely on them. Although recent decades have seen the proliferation of research on aquatic proglacial systems, they have been viewed primarily as conduits between glaciers and downstream systems. Our findings demonstrate that proglacial rivers and estuaries are essential sites for the biogeochemical reworking of glacial DOM, and that glacial DOM signatures may be lost before reaching the coastal interface. As temperatures rise and the distance between glacial termini and coastal interfaces increase, the composition of DOM delivered from glaciers to the ocean via proglacial rivers and estuaries will likely shift with unknown ecosystem impacts. Consequently, we recommend that future research characterize DOM and rates of P-DOM loss within complex proglacial systems globally to better predict and prepare for the biogeochemical impacts of glacial retreat.

## 7.0. TABLES

**Table 1.** Descriptions of location abbreviations used.

<b>Abbreviation</b>	<b>Location</b>	<b>Distance from Terminus (km)</b>	<b>Type</b>
CCI	Central Cook Inlet	250 - 350	seawater
GOA	Gulf of Alaska	500+	seawater
KTA estuary	Knik/Turnagain Arm estuary	100 - 150	brackish
MG	Matanuska Glacier	0	freshwater
MGT	Matanuska Glacier Terminus	0	freshwater
MR	Matanuska River	0 - 100	freshwater
SC AK	Southcentral Alaska	-	-
SE AK	Southeast Alaska	-	-

**Table 2.** Summary of fluorescence peaks and properties. Adapted from Fellman et al. (2010a).

<b>Peak</b>	<b>Resembles</b>	<b>Excitation/emission ranges (nm)</b>	<b>Indicates</b>	<b>Relative bioavailability</b>
B	Protein-like (tyrosine)	ex 270–275, em 304–312	Microbial production	Labile
T	Protein-like (tryptophan)	ex 270–280 (<240), em 330–368	Recent microbial production, potentially intact proteins	Very labile
A	Humic-like	ex 260, em 448–480	Allochthonous (especially forests and wetlands), humic inputs	Recalcitrant
C	Humic-like	ex 320–360, em 420–460	Allochthonous (especially forests and wetlands), humic inputs	Recalcitrant
M	Humic-like	ex 290–325 (,250), em 370–430	Allochthonous (especially marine), humic inputs	Recalcitrant
N	Unknown (red-shifted tryptophan)	ex 280, em 370	Recent phytoplankton production	Very labile

**Table 3.** Summary of major optical parameters excluding fluorescence peaks, which are summarized in Table 1. Adapted from Hansen et al., 2016.

<b>Parameter</b>	<b>Type</b>	<b>Calculated</b>	<b>Purpose</b>
<b>HIX</b>	Fluorescence	The area under the em spectra 435–480 nm divided by the peak area 300–345 nm 1 435–480 nm, at ex 254 nm	An indicator of humic substance content or extent of humification. Higher values indicate an increasing degree of humification.
<b>BIX</b>	Fluorescence	The ratio of emission intensity at 380 nm divided by 430 nm at excitation 310 nm	An indicator of autotrophic productivity. High values (>1) correspond to recently produced DOM of autochthonous origin.
<b>SUVA<sub>254</sub></b>	Absorbance	Absorption coefficient at 254 nm divided by DOC concentration	Absorbance per unit carbon. Typically, a higher number is associated with greater aromatic content.

**Table 4.** Linear model parameters for near-terminus environmental, DOM, and inorganic nutrient variables (See Tables 5-8, Figures 3-7). All linear models included distance from terminus (km) as the predictor variable. Estimates and standard errors are in units of the response variable per km from glacial terminus. Statistically significant *P* values ( $P < 0.050$ ) are italicized.

<b>Response Variable</b>	<b>Distance Estimate</b>	<b>Standard Error</b>	<b>R<sup>2</sup></b>	<b><i>P</i></b>
Specific Conductivity (μS/cm)	14.25	1.49	0.95	<i>2.1 x 10<sup>-4</sup></i>
Alkalinity (mN)	0.05	0.01	0.94	<i>7.2 x 10<sup>-5</sup></i>
Temperature (°C)	0.63	0.07	0.94	<i>3.4 x 10<sup>-4</sup></i>
pH	-0.07	0.01	0.97	<i>7.3 x 10<sup>-5</sup></i>
NO <sub>3</sub> <sup>-</sup> (ng/L)	2510	1234	0.34	0.08
Peak B (QSE)	-0.09	0.09	0.35	0.11
Peak T (QSE)	-0.01	0.01	0.08	0.42
Peak A (QSE)	0.03	0.01	0.59	<i>9.0 x 10<sup>-3</sup></i>
Peak C (QSE)	0.02	0.00	0.65	<i>5.0 x 10<sup>-3</sup></i>
Peak M (QSE)	0.01	0.00	0.45	<i>0.03</i>
Peak N (QSE)	0.01	0.00	0.26	0.13
HIX	0.13	0.04	0.61	<i>7.0 x 10<sup>-3</sup></i>
BIX	-0.04	0.03	0.19	0.22
% Protein-Like DOM	-4.05	0.60	0.85	<i>1.4 x 10<sup>-4</sup></i>

**Table 5.** Major nutrient species in the near-terminus MR. ‘-’ indicates measurements below the limits of detection.

<b>Distance from terminus (km)</b>	<b>Collection Date</b>	<b>DOC (mg L<sup>-1</sup>)</b>	<b>TKN (ng L<sup>-1</sup>)</b>	<b>NO<sub>3</sub><sup>-</sup>-N (ng L<sup>-1</sup>)</b>	<b>DON (ng L<sup>-1</sup>)</b>	<b>TP (ng L<sup>-1</sup>)</b>	<b>DOP (ng L<sup>-1</sup>)</b>	<b>C/N</b>
0	7/16/2019	1.09	1.15x10 <sup>5</sup>	5.38x10 <sup>4</sup>	1.18x10 <sup>5</sup>	9.30x10 <sup>3</sup>	4.17x10 <sup>3</sup>	10.82
0	7/19/2019	1.20	2.00x10 <sup>5</sup>	1.25x10 <sup>4</sup>	2.00x10 <sup>5</sup>	2.04x10 <sup>4</sup>	7.80x10 <sup>3</sup>	7.00
0	7/22/2019	0.53	1.51x10 <sup>5</sup>	-	1.52x10 <sup>5</sup>	5.40x10 <sup>3</sup>	-	4.11
0	7/24/2019	0.70	2.48x10 <sup>5</sup>	-	2.47x10 <sup>5</sup>	2.88x10 <sup>4</sup>	-	3.31
2.22	7/16/2019	0.53	2.05x10 <sup>4</sup>	2.56x10 <sup>4</sup>	2.29x10 <sup>4</sup>	1.50x10 <sup>4</sup>	5.16x10 <sup>3</sup>	26.84
2.22	7/19/2019	0.38	1.56x10 <sup>4</sup>	1.01x10 <sup>4</sup>	1.54x10 <sup>4</sup>	5.10x10 <sup>3</sup>	3.82x10 <sup>3</sup>	28.96
2.22	7/22/2019	0.72	6.72x10 <sup>4</sup>	1.49x10 <sup>4</sup>	6.62x10 <sup>4</sup>	8.70x10 <sup>3</sup>	1.52x10 <sup>3</sup>	12.77
10.63	7/16/2019	0.83	-	5.67x10 <sup>4</sup>	-	-	4.73x10 <sup>3</sup>	-
10.63	7/22/2019	0.55	7.08x10 <sup>4</sup>	2.91x10 <sup>4</sup>	7.07x10 <sup>4</sup>	1.74x10 <sup>4</sup>	4.42x10 <sup>3</sup>	9.02
10.72	7/19/2019	0.94	3.26x10 <sup>5</sup>	4.04x10 <sup>4</sup>	3.27x10 <sup>5</sup>	2.40x10 <sup>3</sup>	3.63x10 <sup>3</sup>	3.34

**Table 6.** Near-terminus fluorescence data. All peak intensities have units of QSE.

<b>Distance from terminus (km)</b>	<b>Collection Date</b>	<b>B</b>	<b>T</b>	<b>A</b>	<b>C</b>	<b>M</b>	<b>N</b>	<b>BIX</b>	<b>HIX</b>
0.02	7/16/2019	4.35	0.72	0.13	0.05	0.08	0.14	0.70	0.11
0.02	7/19/2019	2.98	0.35	0.06	0.02	0.04	0.06	1.67	0.12
0.02	7/22/2019	0.43	0.11	0.06	0.02	0.05	0.06	1.50	0.40
0.02	7/24/2019	0.80	0.13	0.08	0.05	0.13	0.06	0.78	0.50
2.22	7/16/2019	1.53	0.22	0.06	0.02	0.03	0.07	0.42	0.07
2.22	7/19/2019	2.06	0.49	0.18	0.07	0.10	0.18	1.34	0.26
2.22	7/22/2019	0.55	0.22	0.06	0.03	0.04	0.07	1.35	0.33
10.63	7/16/2019	0.91	0.16	0.22	0.11	0.10	0.07	0.50	1.09
10.63	7/22/2019	0.47	0.08	0.25	0.15	0.14	0.16	0.76	2.75
10.72	7/19/2019	1.81	0.36	0.57	0.30	0.30	0.22	0.94	1.02

**Table 7.** %P-DOM in the near-terminus MR.

<b>Distance from terminus (km)</b>	<b>Collection Date</b>	<b>%P-DOM</b>
0.02	7/16/2019	95.12
0.02	7/19/2019	96.54
0.02	7/22/2019	80.88
0.02	7/24/2019	77.96
2.22	7/16/2019	94.19
2.22	7/19/2019	87.71
2.22	7/22/2019	86.17
10.63	7/16/2019	71.26
10.63	7/22/2019	50.37
10.72	7/19/2019	65.04

**Table 8.** Average  $\delta^{13}\text{C}$ -DOC and C/N for the near-terminus MR, riverine endmembers, KTA estuary, and CCI.

<b>System</b>	<b>n</b>	<b>Average <math>\delta^{13}\text{C}</math>-DOC (‰)</b>	<b>Average C/N</b>
Near-terminus MR	3	-27.31	10.20
Riverine endmembers	3	-27.31	10.20
KTA estuary	7	-25.98	13.11
CCI	5	-28.70	12.14

**Table 9.** DOM properties of the Hick’s Creek confluence: the average characteristics of two samples collected directly upstream of the confluence, characteristics of Hick’s Creek itself, and characteristics of the sample site directly downstream of the confluence. All peak intensities have units of QSE. See Figure 1 for location of Hicks Creek.

<b>Relative Position</b>	<b>ID</b>	<b>Distance from terminus (km)</b>	<b>TOC</b>	<b>B</b>	<b>T</b>	<b>A</b>	<b>C</b>	<b>M</b>	<b>N</b>	<b>BIX</b>	<b>HIX</b>	<b>%P-DOM</b>
Upstream	MM1_Average	10.63	0.69	0.69	0.12	0.23	0.13	0.12	0.12	0.63	1.92	24.48
Tributary	HPC	10.69	3.11	1.56	0.66	2.44	1.23	1.11	0.74	0.62	3.50	31.69
Downstream	MR&HPC	10.72	0.94	1.81	0.36	0.57	0.30	0.30	0.22	0.94	1.02	37.14

**Table 10.** Nutrients for KTA estuary in order of increasing salinity. ‘-’ indicates measurements below the limits of detection. ‘NA’ indicated data was excluded as outliers (see Results).

Salinity (PSU)	Site	NH <sub>3</sub> (ng L <sup>-1</sup> )	NO <sub>3</sub> <sup>-</sup> -N (ng L <sup>-1</sup> )	DON (ng L <sup>-1</sup> )	DOC (mg L <sup>-1</sup> )	C/N
5.47	KTA 1	-	6.11x10 <sup>4</sup>	2.84x10 <sup>5</sup>	1.10	4.53
7.93	KTA 3	4.44x10 <sup>3</sup>	4.83x10 <sup>4</sup>	1.17x10 <sup>5</sup>	1.10	10.99
8.22	KTA 2	6.04x10 <sup>3</sup>	1.03x10 <sup>5</sup>	1.60x10 <sup>5</sup>	1.40	10.16
9.00	KTA 1	1.64x10 <sup>3</sup>	6.45x10 <sup>4</sup>	1.16x10 <sup>5</sup>	1.10	11.10
9.31	KTA 2	6.64x10 <sup>3</sup>	5.48x10 <sup>4</sup>	NA	NA	NA
10.06	KTA 5	6.65x10 <sup>4</sup>	8.97x10 <sup>4</sup>	9.04x10 <sup>4</sup>	1.07	13.77
12.71	KTA 4	-	1.08x10 <sup>5</sup>	9.38x10 <sup>4</sup>	1.85	23.07

**Table 11.** Linear model parameter estimates for estuarine system variables and salinity (PSU; see Tables 10-12, Figure 10). Estimates and standard errors are in units of the response variable per PSU. Statistically significant  $P$  values ( $P < 0.050$ ) are italicized.

<b>Response Variable</b>	<b>Salinity Estimate</b>	<b>Standard Error</b>	<b>R<sup>2</sup></b>	<b><i>P</i></b>
DOC (mg/L)	0.09	0.05	0.36	0.16
DON (ng/L)	-0.03	0.01	0.45	0.08
C/N	2.48	0.26	0.96	<i>6.4 x 10<sup>-4</sup></i>
Peak N (QSE)	-0.07	0.02	0.74	<i>0.01</i>
Peak C (QSE)	-0.10	0.03	0.74	<i>0.01</i>
Peak M (QSE)	-0.10	0.02	0.81	<i>6.0 x 10<sup>-3</sup></i>
HIX	-0.40	0.44	0.14	0.41
BIX	-0.04	0.02	0.60	<i>0.04</i>
SUVA <sub>254</sub> (L mg C <sup>-1</sup> m <sup>-1</sup> )	-0.30	0.15	0.43	0.11

**Table 12.** Optical properties for KTA estuary in order of increasing salinity. All peak intensities are in units of QSE.

<b>Salinity</b>	<b>Site</b>	<b>B</b>	<b>T</b>	<b>A</b>	<b>C</b>	<b>M</b>	<b>N</b>	<b>BIX</b>	<b>HIX</b>	<b>% P-DOM</b>	<b>SUVA<sub>254</sub> (L mg C<sup>-1</sup> m<sup>-1</sup>)</b>
5.47	KTA 1	0.97	0.49	1.39	1.02	1.03	0.78	0.77	3.98	29.71	3.29
7.93	KTA 3	1.19	0.30	0.49	0.83	0.75	0.51	0.83	7.03	41.93	2.52
8.22	KTA 2	0.98	0.42	2.17	0.79	0.69	0.50	0.59	2.53	27.76	2.25
9.00	KTA 1	1.66	0.40	1.48	0.46	0.43	0.31	0.62	2.16	46.62	1.61
9.31	KTA 2	0.85	0.49	1.60	0.72	0.67	0.54	0.64	3.22	30.92	3.50
10.06	KTA 5	0.48	0.26	0.92	0.79	0.69	0.49	0.69	6.63	23.70	2.93
12.71	KTA 4	0.54	0.47	1.46	0.24	0.22	0.23	0.46	0.76	34.50	0.67

**Table 13.** Major nutrient concentrations for riverine endmembers feeding the KTA estuary. ‘-’ indicates measurements below the limits of detection. See Figure 1 for site locations.

<b>River</b>	<b>Date</b>	<b>NH<sub>3</sub> (ng L<sup>-1</sup>)</b>	<b>NO<sub>3</sub><sup>-</sup>-N</b>	<b>DOC</b>	<b>DON</b>
Matanuska/Knik	7/18/2019	-	5.50x10 <sup>4</sup>	0.90	2.37x10 <sup>4</sup>
Matanuska/Knik	7/20/2019	-	6.77x10 <sup>4</sup>	0.65	1.15x10 <sup>5</sup>
Matanuska/Knik	7/23/2019	3.54x10 <sup>3</sup>	1.56x10 <sup>4</sup>	0.44	-
20 Mile	7/22/2019	1.66x10 <sup>3</sup>	2.80x10 <sup>4</sup>	0.66	1.98x10 <sup>5</sup>
20 Mile	7/25/2019	1.70x10 <sup>2</sup>	-	0.33	-
Portage	7/22/2019	-	4.20x10 <sup>4</sup>	0.72	2.90x10 <sup>5</sup>
Portage	7/25/2019	-	3.17x10 <sup>4</sup>	0.35	-
Placer	7/22/2019	-	2.11x10 <sup>4</sup>	0.42	1.33x10 <sup>4</sup>
Placer	7/25/2019	-	-	0.61	1.03x10 <sup>5</sup>
<b>Average</b>		<b>5.97x10<sup>2</sup></b>	<b>2.90x10<sup>4</sup></b>	<b>0.57</b>	<b>8.20x10<sup>4</sup></b>

**Table 14.** DOM parameters for riverine endmembers of the KTA estuary. All peak intensities are in units of QSE. See Figure 1 for site locations.

<b>River</b>	<b>Date</b>	<b>B</b>	<b>T</b>	<b>A</b>	<b>C</b>	<b>M</b>	<b>N</b>	<b>BIX</b>	<b>HIX</b>	<b>SUVA<sub>254</sub> (L mg C<sup>-1</sup> m<sup>-1</sup>)</b>	<b>%P-DOM</b>
Matanuska/Knik	7/18/2019	2.05	0.26	0.60	0.30	0.31	0.22	0.78	1.07	0.51	65.71
Matanuska/Knik	7/20/2019	2.25	0.45	0.57	0.27	0.30	0.27	0.70	0.80	0.82	70.47
Matanuska/Knik	7/23/2019	0.51	0.13	0.19	0.12	0.12	0.13	1.17	1.47	1.26	59.88
20 Mile	7/22/2019	0.98	0.18	0.30	0.15	0.13	0.12	0.20	0.68	1.43	66.98
20 Mile	7/25/2019	0.34	0.10	0.24	0.14	0.12	0.11	0.45	2.18	1.89	46.93
Portage	7/22/2019	0.84	0.19	0.29	0.16	0.13	0.13	0.46	1.31	3.11	64.07
Portage	7/25/2019	0.32	0.14	0.26	0.15	0.13	0.15	0.91	2.14	1.23	45.70
Placer	7/22/2019	0.47	0.13	0.13	0.08	0.06	0.07	0.68	1.03	0.80	68.84
Placer	7/25/2019	0.29	0.11	0.14	0.08	0.07	0.08	0.57	0.94	1.33	58.05
<b>Average</b>		<b>0.89</b>	<b>0.19</b>	<b>0.30</b>	<b>0.16</b>	<b>0.15</b>	<b>0.14</b>	<b>0.66</b>	<b>1.29</b>	<b>1.38</b>	<b>60.74</b>

**Table 15.** Notable nutrients of CCI at 5 and 30m depths. ‘-’ indicates measurements below the limits of detection.

Site	Collection Date	Depth (m)	NH <sub>3</sub> (ng L <sup>-1</sup> )	NO <sub>3</sub> <sup>-</sup> -N (ng L <sup>-1</sup> )	DON (ng L <sup>-1</sup> )	TP (ng L <sup>-1</sup> )	OP (ng L <sup>-1</sup> )	DOC (mg L <sup>-1</sup> )	C/N
CCI 1	7/23/2019	5	1.24x10 <sup>4</sup>	8.80x10 <sup>4</sup>	4.03x10 <sup>5</sup>	2.88x10 <sup>4</sup>	9.20x10 <sup>3</sup>	1.30	3.77
CCI 1	7/24/2019	5	1.14x10 <sup>4</sup>	7.27x10 <sup>4</sup>	2.87x10 <sup>5</sup>	1.83x10 <sup>4</sup>	8.24x10 <sup>3</sup>	1.62	6.59
CCI 2	7/23/2019	5	3.84x10 <sup>3</sup>	6.89x10 <sup>4</sup>	2.02x10 <sup>5</sup>	6.30x10 <sup>4</sup>	6.31x10 <sup>3</sup>	1.34	7.72
CCI 2	7/24/2019	5	7.64x10 <sup>3</sup>	7.04x10 <sup>4</sup>	3.65x10 <sup>4</sup>	4.71x10 <sup>4</sup>	2.64x10 <sup>3</sup>	1.26	40.37
CCI 3	7/24/2019	5	2.60x10 <sup>4</sup>	7.33x10 <sup>4</sup>	7.93x10 <sup>4</sup>	9.30x10 <sup>3</sup>	-	1.57	23.10
CCI 3	7/23/2019	5	1.61x10 <sup>4</sup>	5.68x10 <sup>4</sup>	2.80x10 <sup>4</sup>	4.17x10 <sup>4</sup>	-	1.34	56.05
CCI 4	7/24/2019	5	8.54x10 <sup>3</sup>	6.17x10 <sup>4</sup>	9.77x10 <sup>4</sup>	1.92x10 <sup>4</sup>	2.38x10 <sup>3</sup>	1.16	13.91
CCI 4	7/23/2019	5	1.09x10 <sup>4</sup>	7.64x10 <sup>4</sup>	1.65x10 <sup>5</sup>	2.43x10 <sup>4</sup>	3.76x10 <sup>3</sup>	1.36	9.61
CCI 5	7/23/2019	5	2.92x10 <sup>4</sup>	9.70x10 <sup>4</sup>	2.51x10 <sup>4</sup>	3.57x10 <sup>4</sup>	8.10x10 <sup>3</sup>	1.89	88.01
CCI 5	7/24/2019	5	1.12x10 <sup>4</sup>	7.01x10 <sup>4</sup>	3.95x10 <sup>5</sup>	9.90x10 <sup>3</sup>	-	2.04	6.02
CCI 1	7/23/2019	30	1.19x10 <sup>4</sup>	6.89x10 <sup>4</sup>	1.58x10 <sup>5</sup>	1.86x10 <sup>4</sup>	5.38x10 <sup>3</sup>	1.66	12.29
CCI 1	7/24/2019	30	5.34x10 <sup>3</sup>	8.85x10 <sup>4</sup>	1.03x10 <sup>5</sup>	2.07x10 <sup>4</sup>	6.56x10 <sup>3</sup>	1.34	15.24
CCI 2	7/23/2019	30	-	7.31x10 <sup>4</sup>	3.02x10 <sup>5</sup>	4.68x10 <sup>4</sup>	8.74x10 <sup>3</sup>	1.38	5.19
CCI 2	7/24/2019	30	1.60x10 <sup>4</sup>	8.11x10 <sup>4</sup>	1.53x10 <sup>5</sup>	2.40x10 <sup>3</sup>	-	1.35	10.26
CCI 3	7/24/2019	30	3.85x10 <sup>4</sup>	1.50x10 <sup>5</sup>	3.14x10 <sup>5</sup>	1.59x10 <sup>4</sup>	8.70x10 <sup>3</sup>	1.36	5.06
CCI 3	7/23/2019	30	2.74x10 <sup>4</sup>	8.46x10 <sup>4</sup>	3.34x10 <sup>5</sup>	1.39x10 <sup>5</sup>	7.20x10 <sup>2</sup>	1.66	5.78
CCI 4	7/24/2019	30	3.20x10 <sup>4</sup>	5.50x10 <sup>4</sup>	2.33x10 <sup>5</sup>	6.81x10 <sup>4</sup>	6.50x10 <sup>3</sup>	1.60	8.00
CCI 4	7/23/2019	30	1.92x10 <sup>4</sup>	3.85x10 <sup>4</sup>	1.08x10 <sup>4</sup>	3.81x10 <sup>4</sup>	9.80x10 <sup>2</sup>	1.11	120.17
CCI 5	7/24/2019	30	9.84x10 <sup>3</sup>	4.95x10 <sup>4</sup>	1.43x10 <sup>5</sup>	5.94x10 <sup>4</sup>	-	1.64	13.45
CCI 5	7/23/2019	30	3.95x10 <sup>4</sup>	5.20x10 <sup>4</sup>	1.18x10 <sup>5</sup>	5.19x10 <sup>4</sup>	5.67x10 <sup>3</sup>	1.40	13.85

**Table 16.** Notable optical properties of CCI at 5 and 30m depths. All peak intensities have units of QSE.

<b>Site</b>	<b>Collection Date</b>	<b>Depth (m)</b>	<b>B</b>	<b>A</b>	<b>T</b>	<b>C</b>	<b>M</b>	<b>N</b>	<b>BIX</b>	<b>HIX</b>	<b>%P-DOM</b>
CCI 1	7/23/2019	5	0.61	0.46	0.49	0.44	0.48	0.44	0.79	3.57	44.23
CCI 1	7/24/2019	5	0.49	0.97	0.33	0.22	0.24	0.21	0.88	1.32	36.40
CCI 2	7/23/2019	5	0.40	0.76	0.16	0.46	0.44	0.25	0.91	3.94	25.30
CCI 2	7/24/2019	5	0.40	0.77	0.33	0.49	0.50	0.36	0.69	3.63	29.17
CCI 3	7/24/2019	5	0.52	0.60	0.34	0.32	0.31	0.15	0.73	1.90	40.94
CCI 3	7/23/2019	5	0.59	0.66	0.67	0.39	0.37	0.36	0.64	2.08	46.91
CCI 4	7/24/2019	5	0.34	0.66	0.10	0.31	0.31	0.19	0.87	3.27	25.65
CCI 4	7/23/2019	5	0.44	0.70	0.12	0.38	0.38	0.23	0.83	3.46	27.77
CCI 5	7/23/2019	5	0.85	0.76	0.12	0.37	0.36	0.22	0.53	3.00	39.40
CCI 5	7/24/2019	5	1.17	0.83	0.26	0.25	0.26	0.17	0.94	2.21	51.71
CCI 1	7/23/2019	30	0.48	0.92	0.41	0.31	0.35	0.30	1.08	2.22	36.32
CCI 1	7/24/2019	30	0.33	0.88	0.24	0.34	0.38	0.31	0.53	2.83	26.22
CCI 2	7/23/2019	30	0.48	0.66	0.35	0.26	0.30	0.35	0.86	2.54	40.65
CCI 2	7/24/2019	30	0.49	0.63	0.30	0.34	0.39	0.22	0.84	3.40	36.64
CCI 3	7/24/2019	30	0.35	0.72	0.13	0.25	0.25	0.21	0.60	2.14	28.19
CCI 3	7/23/2019	30	0.53	0.52	0.23	0.36	0.34	0.16	0.83	1.86	38.72
CCI 4	7/24/2019	30	0.57	0.47	0.80	0.36	0.45	0.44	0.70	1.29	51.69
CCI 4	7/23/2019	30	0.67	0.48	0.43	0.31	0.36	0.34	0.79	2.63	49.11
CCI 5	7/24/2019	30	0.33	0.58	0.98	0.38	0.52	0.63	0.91	1.10	46.98
CCI 5	7/23/2019	30	0.36	0.45	0.24	0.24	0.25	0.09	0.79	2.09	39.02

**Table 17.** ANOVA and Tukey HSD tests indicated that the KTA estuary is elevated in the listed parameters relative to the riverine endmembers.

<b>Parameter</b>	<b>ANOVA</b>		<b>Tukey HSD</b>	
	<b>F-value</b>	<b><i>P</i></b>	<b>Difference</b>	<b><i>P</i></b>
NO <sub>3</sub> <sup>-</sup>	11.53	1.00x10 <sup>-4</sup>	4.41x10 <sup>4</sup> ng L <sup>-1</sup>	2.22x10 <sup>-3</sup>
DOC	43.32	5.90x10 <sup>-10</sup>	0.65 mg L <sup>-1</sup>	1.87x10 <sup>-5</sup>
Peak A	30.81	2.83x10 <sup>-8</sup>	1.05 QSE	1.87x10 <sup>-5</sup>
Peak C	34.06	9.46x10 <sup>-9</sup>	0.54 QSE	1.87x10 <sup>-5</sup>
Peak M	26.10	1.60x10 <sup>-7</sup>	0.49 QSE	1.00x10 <sup>-7</sup>
Peak N	14.27	3.43x10 <sup>-5</sup>	0.34 QSE	1.99x10 <sup>-5</sup>
HIX	8.31	1.20x10 <sup>-3</sup>	0.25 QSE	8.00x10 <sup>-4</sup>
SUVA <sub>254</sub>	5.98	1.72x10 <sup>-7</sup>	1.02 L mg C <sup>-1</sup> m <sup>-1</sup>	5.17x10 <sup>-3</sup>

**Table 18.** Tukey HSD tests indicated that the KTA estuary is elevated in the listed parameters relative to the CCI (see Table 13 for ANOVA results for the listed parameters). Negative differences indicate that the KTA has higher values than the CCI.

<b>Parameter</b>	<b>Tukey HSD</b>	
	<b>Difference</b>	<b><i>P</i></b>
Peak A	-0.68 QSE	5.40x10 <sup>-6</sup>
Peak C	-0.36 QSE	1.50x10 <sup>-7</sup>
Peak M	-0.28 QSE	1.24x10 <sup>-3</sup>
SUVA <sub>254</sub>	-0.72 L mg C <sup>-1</sup> m <sup>-1</sup>	2.63x10 <sup>-2</sup>

**Table 19.** Near-terminus cross-study comparison location and sampling information.

<b>Study</b>	<b>Location</b>	<b>Climate characteristics</b>	<b>Sample season</b>	<b>Range of distances (km)</b>	<b>n</b>	<b>%P-DOM Method</b>
Fellman et al. (2010)	SE AK	Maritime (high precipitation, relatively mild)	Peak melt: June	6.94 - 12.09	3	PARAFAC
Hood et al. (2009)	SE AK; SC AK	SE AK: maritime; SC AK: maritime	Peak melt: July	SE AK: 6.9 - 11.2; SC AK: 5.7 - 22.0	SE AK: 2; SC AK: 5	PARAFAC
Sussman	SC AK	Maritime/transitional (less precipitation and more variable temperatures than maritime)	Peak melt: July	0.02 - 22	16	Peak picking
Zhou et al. (2019)	Himalayas	Continental (arid, summer monsoon season, cold)	Peak melt: August	0.01 - 26.55	34	PARAFAC

**Table 20.** Linear model parameters for near-terminus cross-study comparison of %P-DOM and distance (see Table 19; Figure 18). Estimate and standard error show the change in %P-DOM per km from glacial terminus. Statistically significant *P* values ( $P < 0.050$ ) are italicized.

<b>Location</b>	<b>Reference(s)</b>	<b>Distance Estimate</b>	<b>Standard Error</b>	<b>R<sup>2</sup></b>	<b><i>P</i></b>
Himalayas	Zhou et al. (2019)	-1.33	0.19	0.62	<i>7.9 x 10<sup>-8</sup></i>
SC Alaska	Hood et al. (2009)	-2.41	1.16	0.59	0.13
SE Alaska	Fellman et al. (2014); Hood et al. (2009)	-2.94	0.64	0.88	<i>0.02</i>

## 8.0. FIGURES

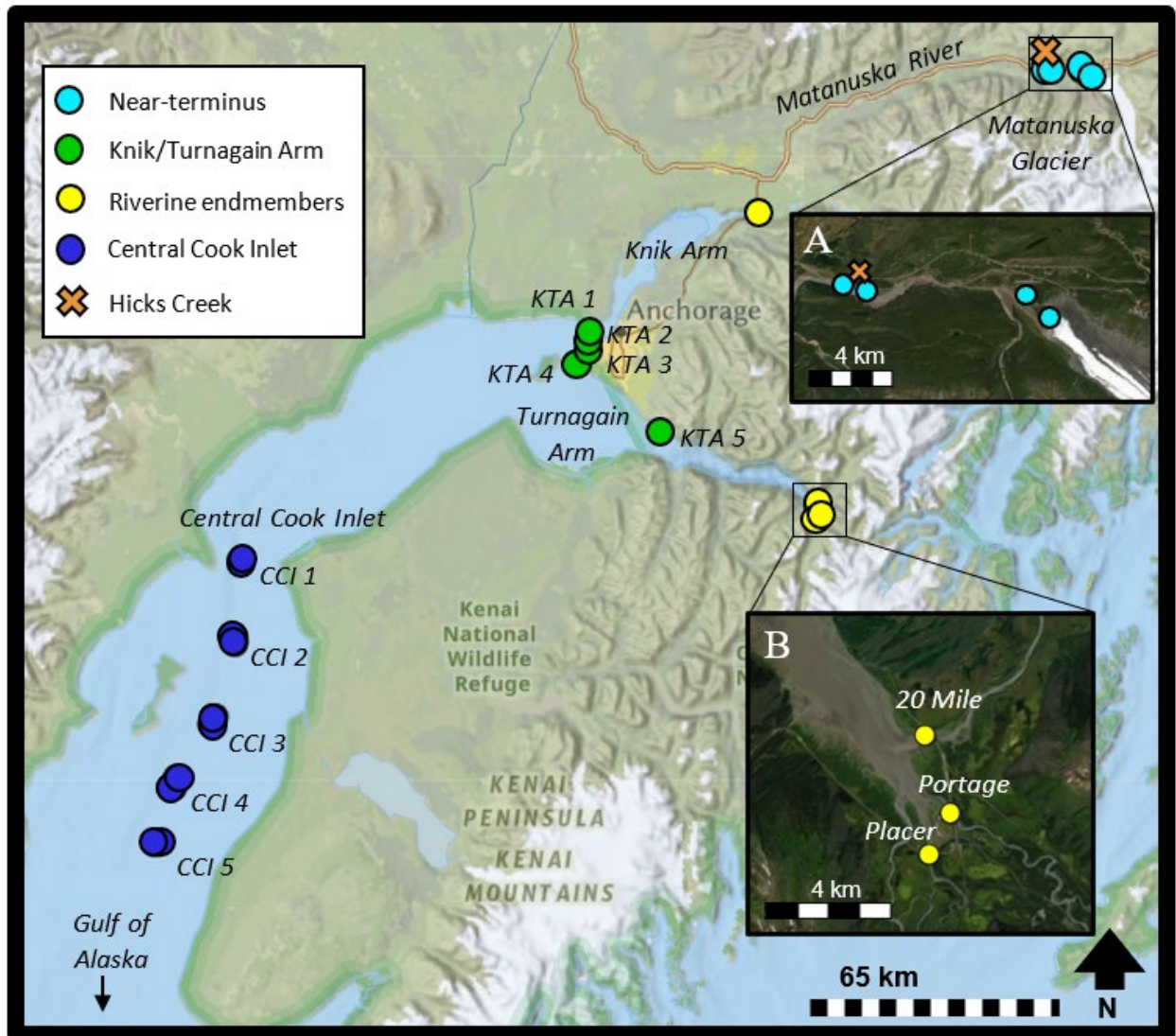


**Figure 1.** Map of the Matanuska Glacier system in SC AK. Near-terminus samples are in located displayed as light blue circles, riverine endmembers are displayed as yellow circles, KTA estuary samples are displayed as green circles (labeled KTA 1 – 5 based on north-south positions), Central Cook Inlet samples are displayed as blue circles (labeled CCI 1 – 5 based on north-south positions), and Hicks Creek is displayed as an orange cross. A) shows the near-terminus sites and B) shows the Portage, Placer, and 20 Mile sample sites.

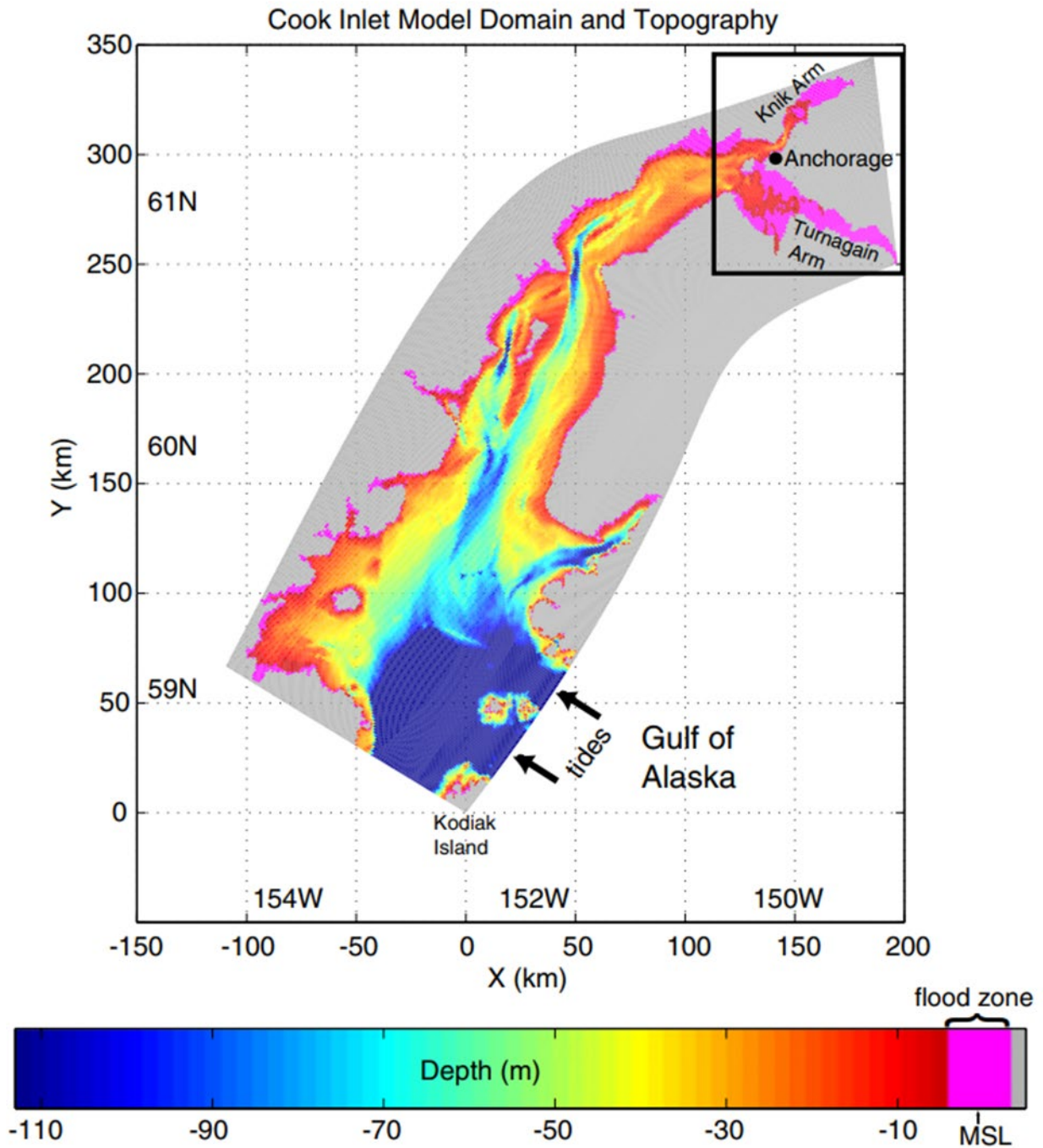


**Figure 2.** Cook Inlet model topography. Depth relative to the local mean sea level is indicated by the blue to red color scale. Gray areas are dry land. Magenta areas are tidally inundated. the boxed region is the KTA estuary. Adapted from Oey et al. (2007) by Ezer & Liu (2010).

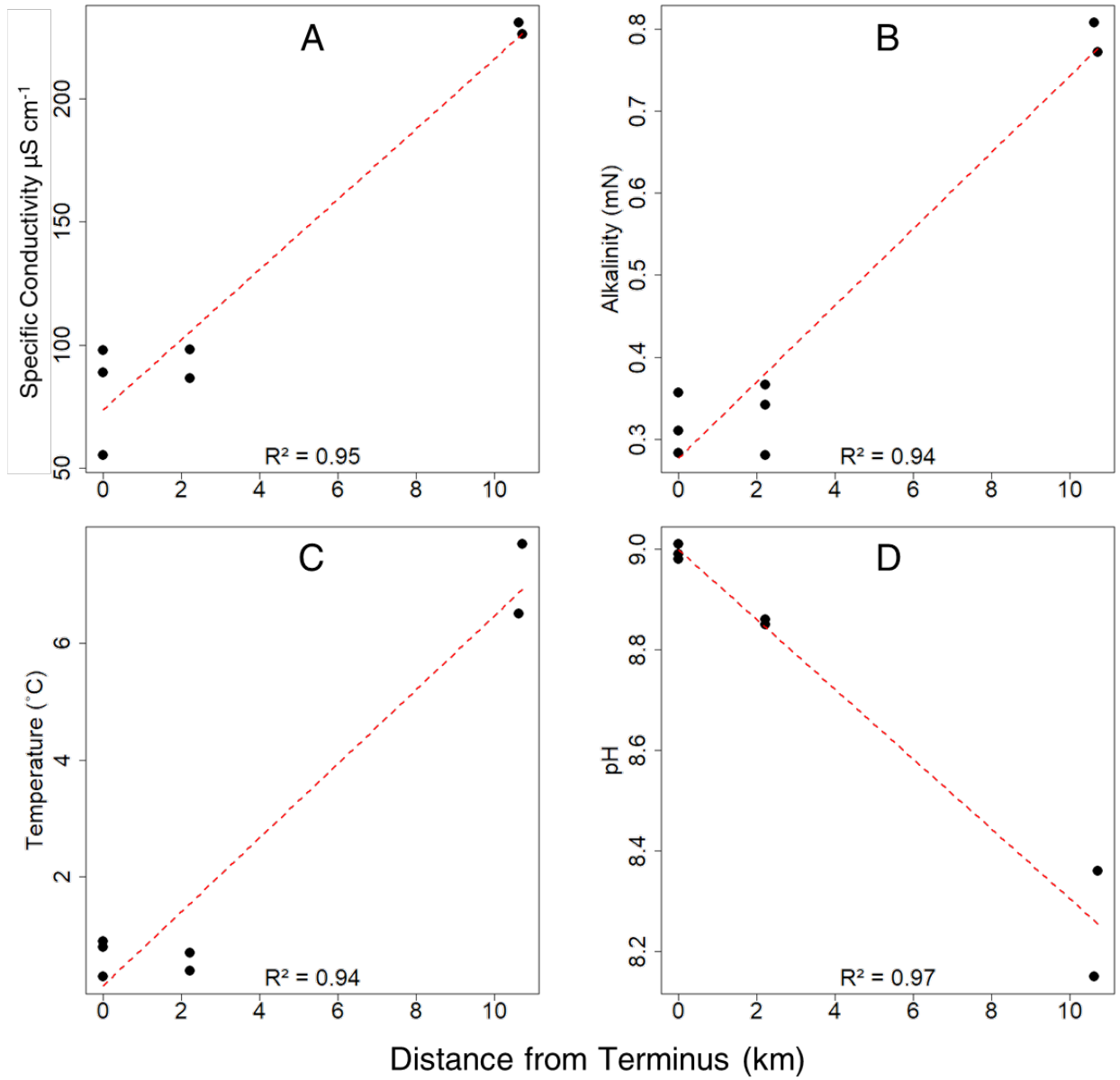


**Figure 3.** Near-terminus environmental parameters over the initial 11 km transect: specific conductivity (A), alkalinity (B), temperature (C), and pH (D).

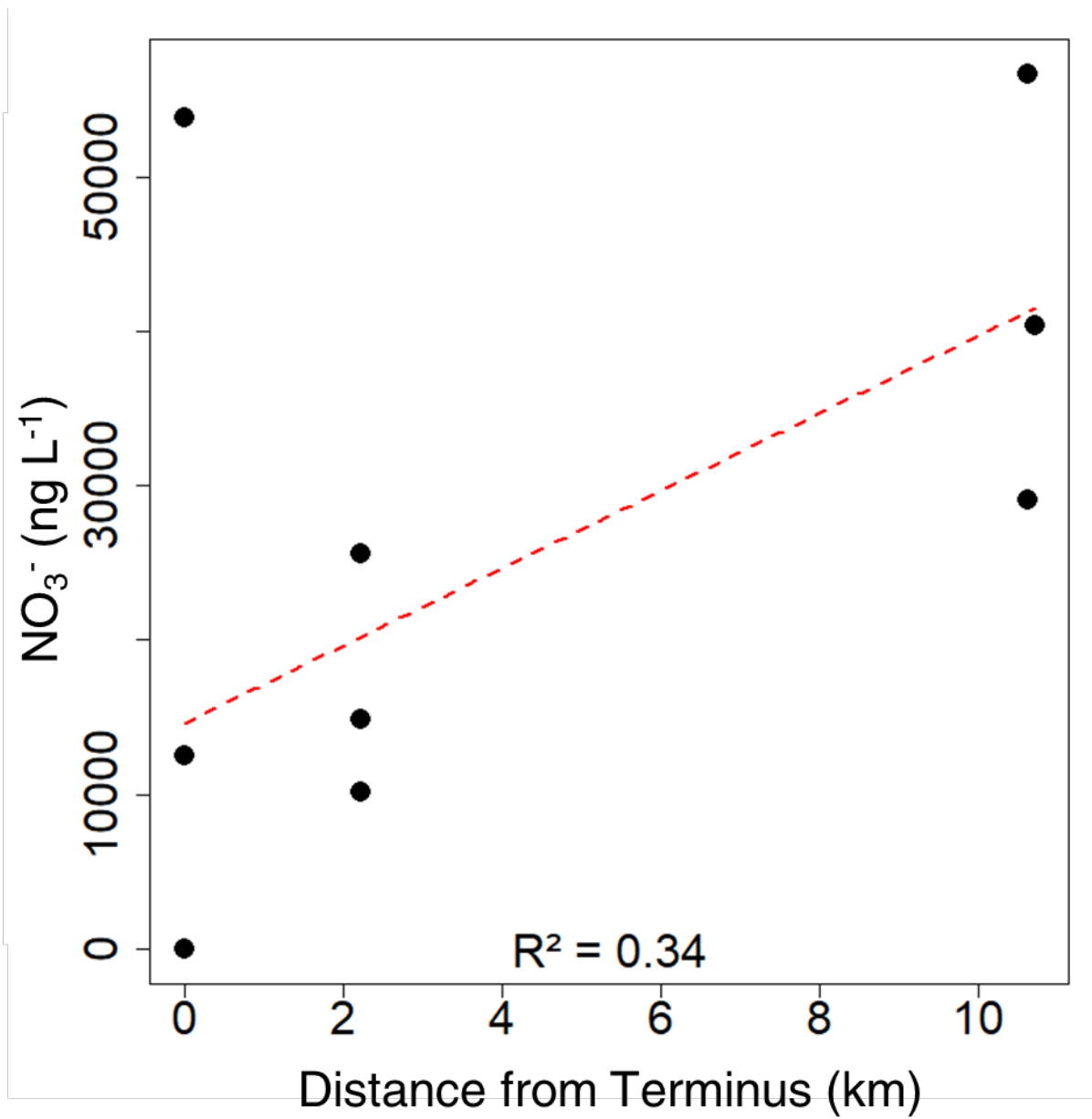


**Figure 4.**  $\text{NO}_3^-$  tends to increase over the 11 km near-terminus transect.

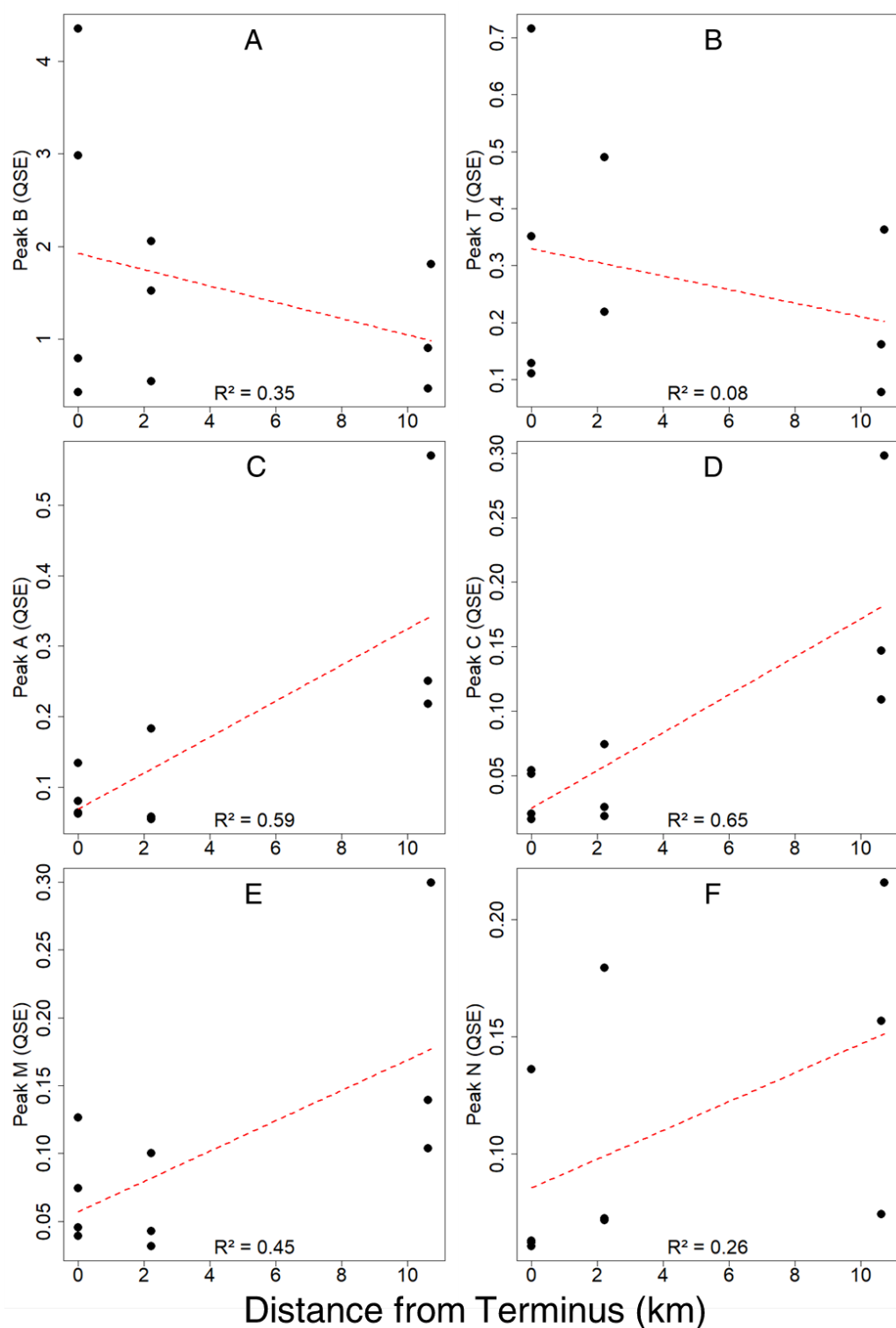


**Figure 5.** Fluorescence peaks versus distance from terminus for near-terminus DOM including protein-like peak B (A) and peak T (B); humic-like peak A (C), peak C (D), and peak M (E); and peak N (F).

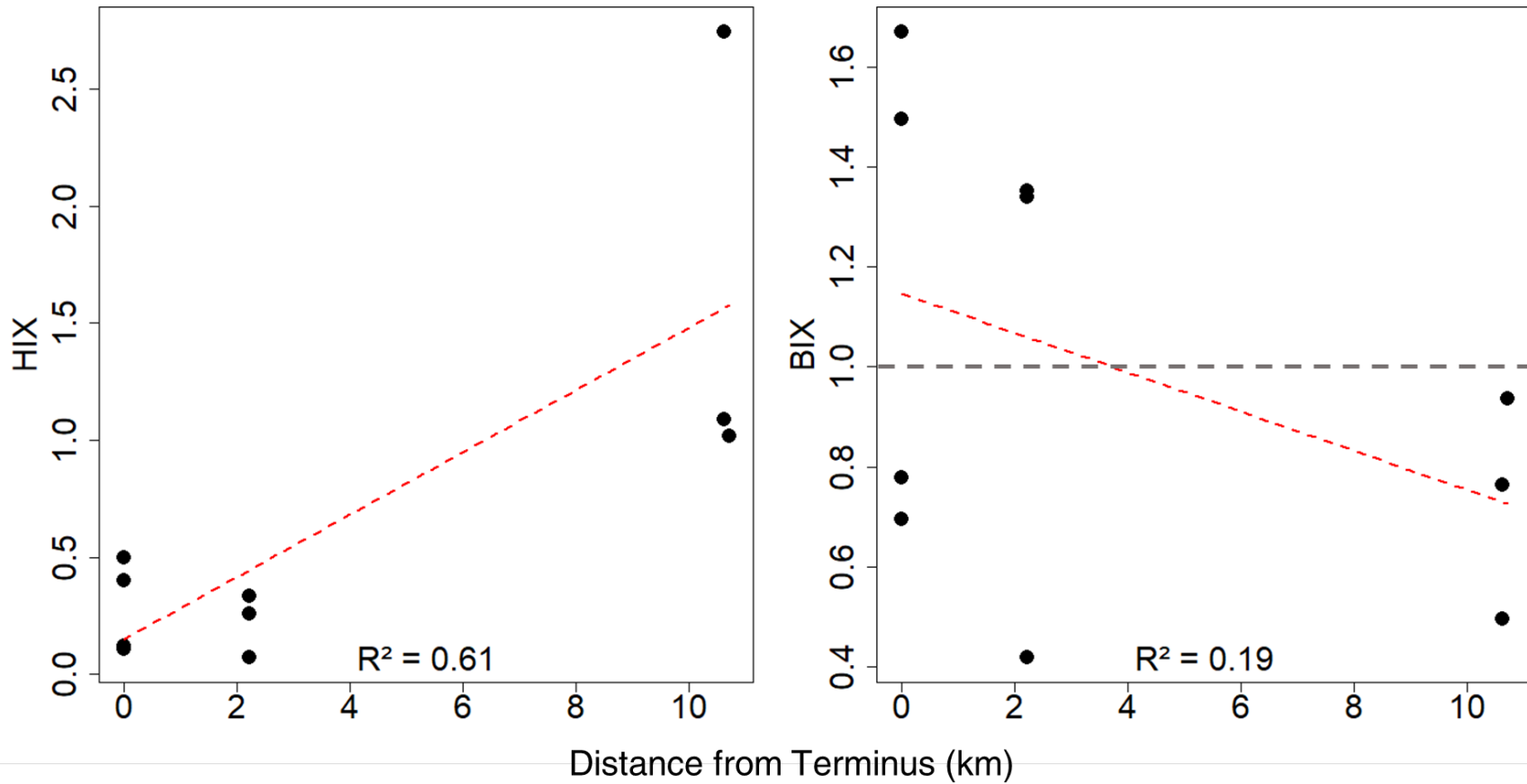


**Figure 6.** HIX (A) and BIX (B) versus distance from the terminus. A BIX value > 1.00 (dotted gray line) indicates recent autochthonous production.

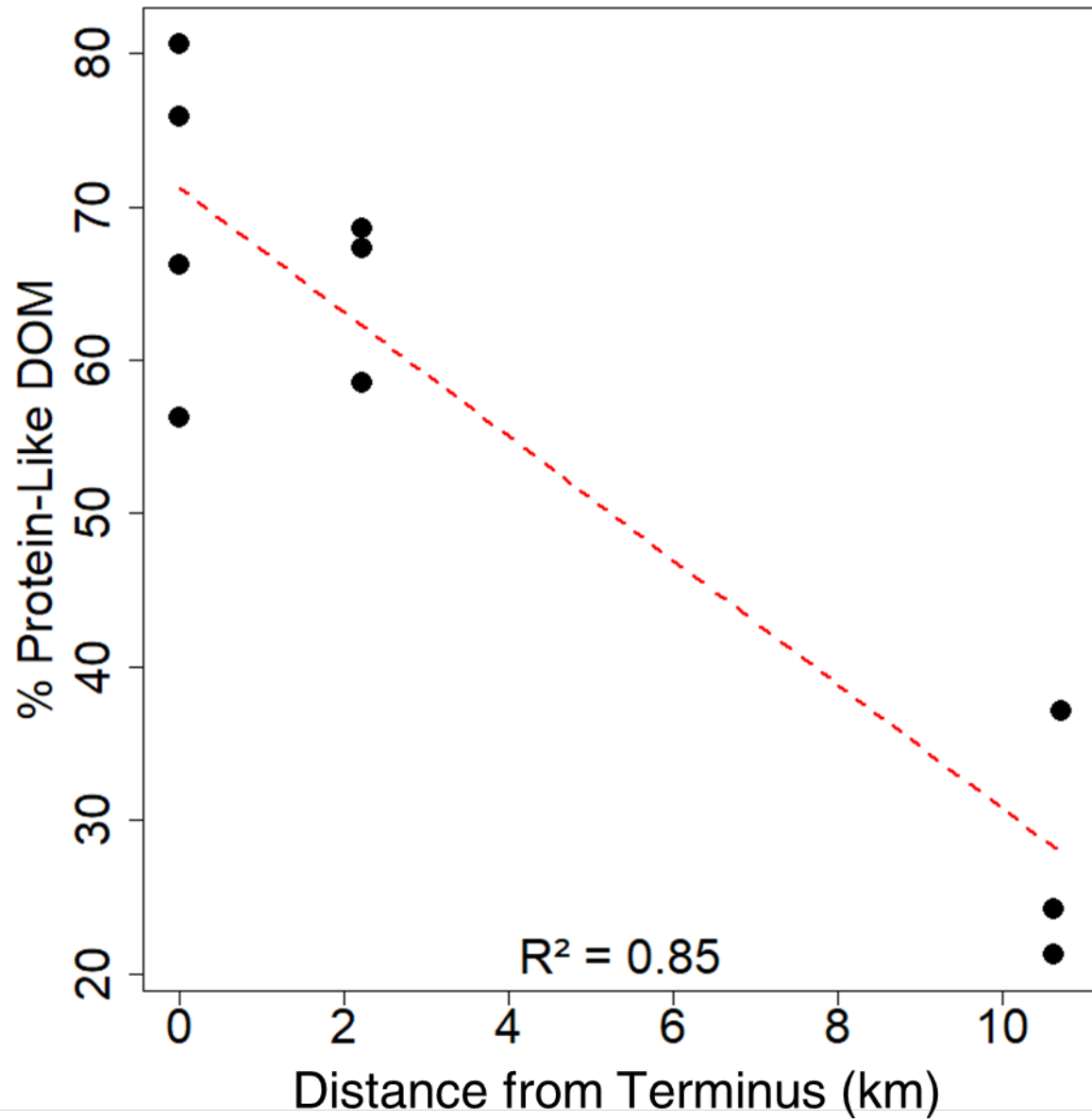


**Figure 7.** %P-DOM vs distance from terminus. %P-DOM decreases significantly over the 11 km transect.

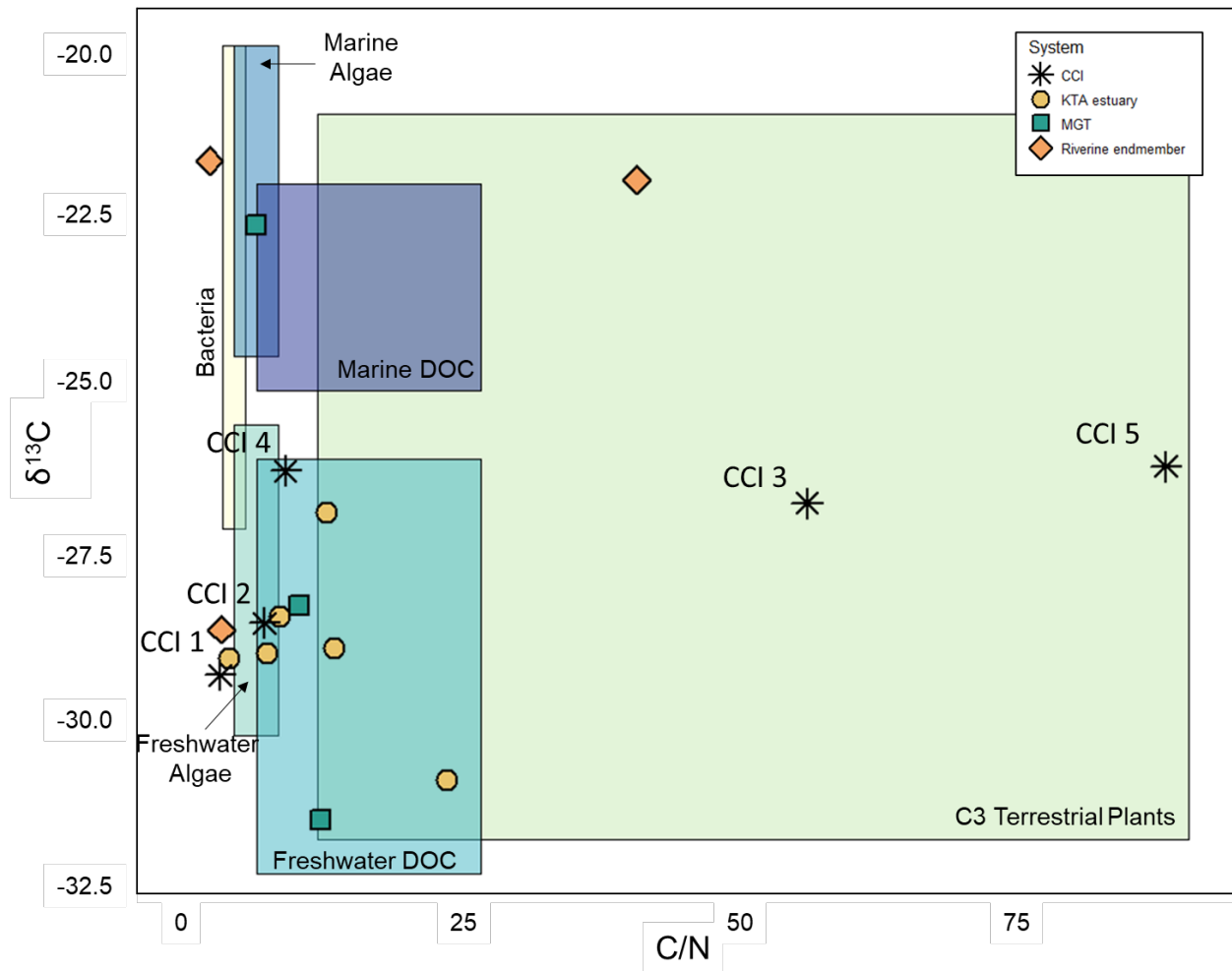


**Figure 8.**  $\delta^{13}\text{C}$  versus C/N with corresponding DOM source materials in shaded boxes (adapted from Lamb et al., 2006).

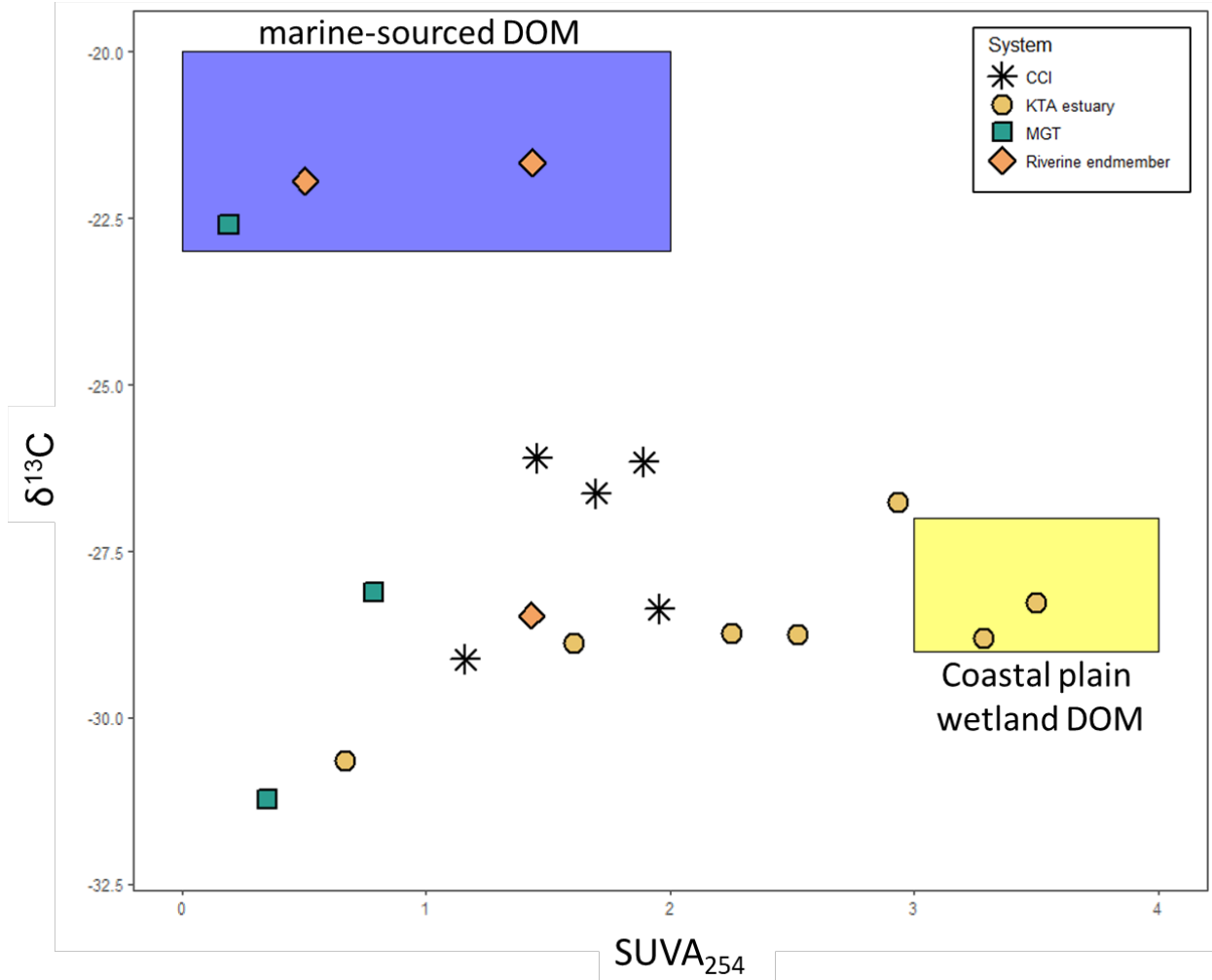


**Figure 9.**  $\delta^{13}\text{C}$  versus  $\text{SUVA}_{254}$  for the Matanuska Glacier system. The light blue shaded box represents marine-source DOM (Raymond and Bauer, 2001a; Helms et al., 2008). The light-yellow shaded box represents coastal plain wetlands (Vähätalo and Wetzel 2008; Opsahl et al. 2005; Hall et al., 2008). Adapted from Rudolph et al. (2020).

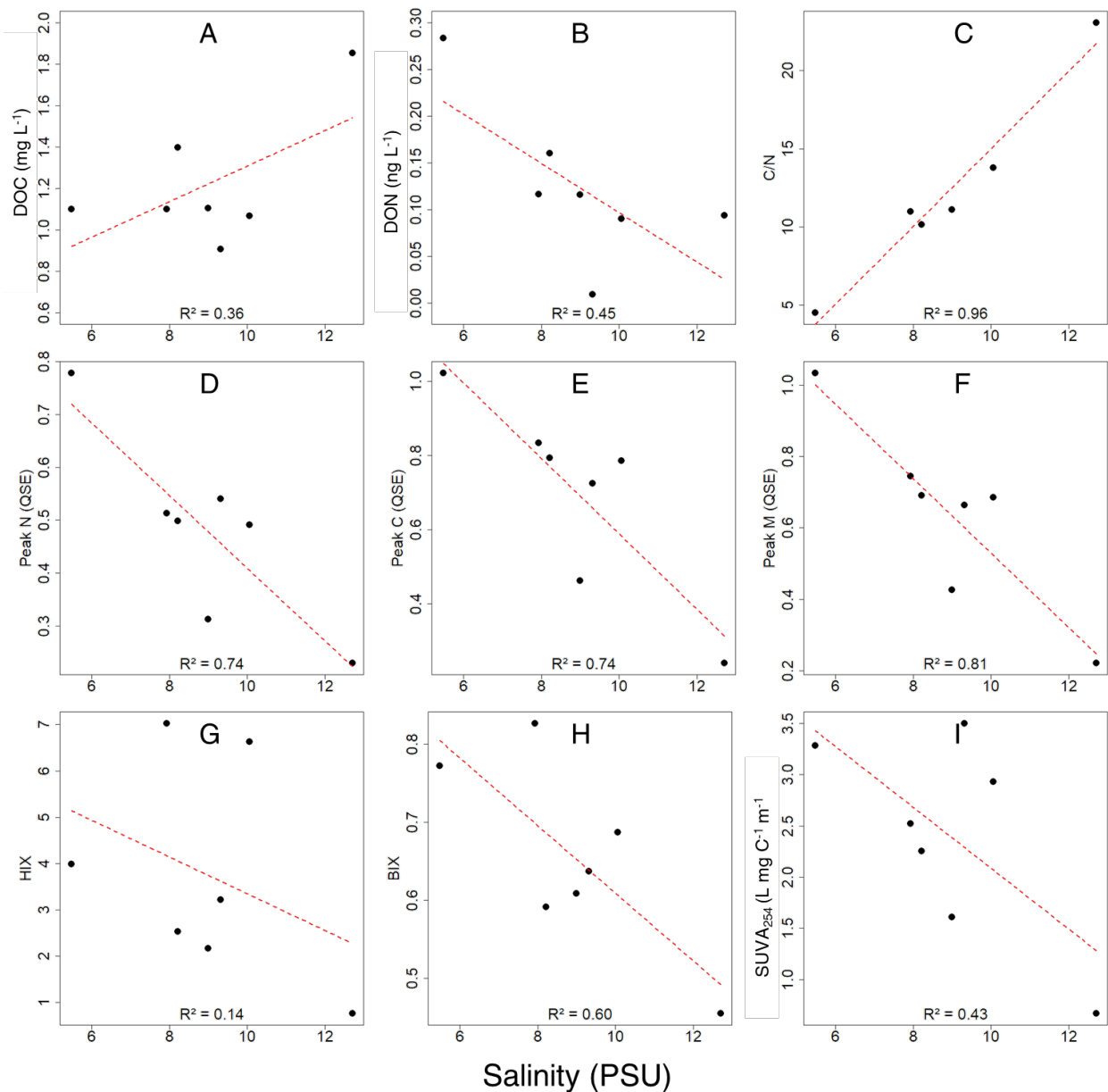


**Figure 10.** DOC (A), DON (B), and C/N (C); humic-like peaks with peak N (D), peak C (E), and peak M (F); HIX (G) and BIX (G; all estuarine BIX values < 1.00); and SUVA<sub>254</sub> (I), all vs salinity (PSU) in the KTA estuary. DON, Peak N, Peak C, Peak M, and BIX decrease with increasing salinity ( $P < 0.05$  for all), and C/N increases with salinity ( $P = 0.013$ ).

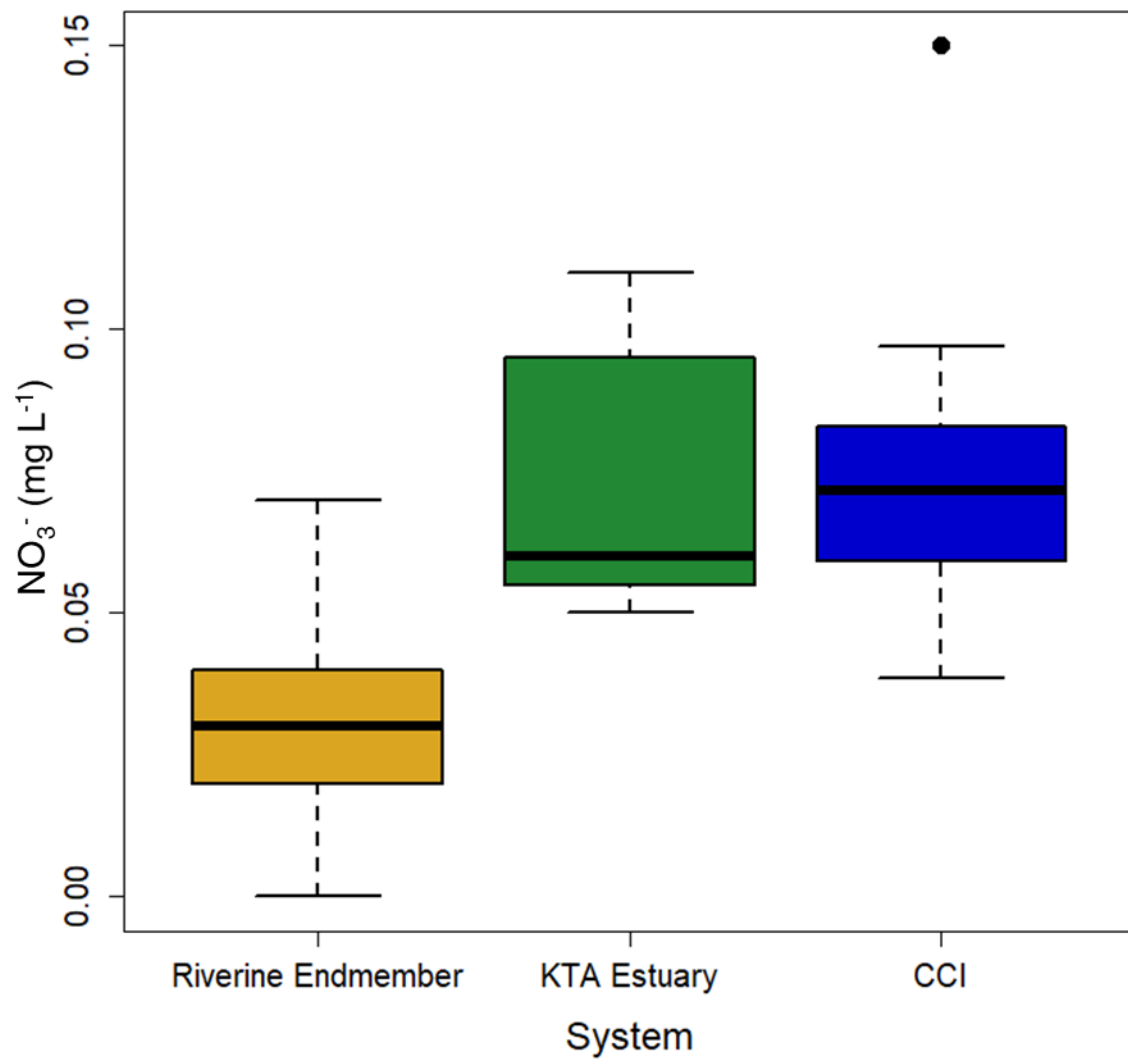


**Figure 11.** Boxplot of the range and median for  $\text{NO}_3^-$  in the riverine endmembers, the KTA estuary, and the CCI.

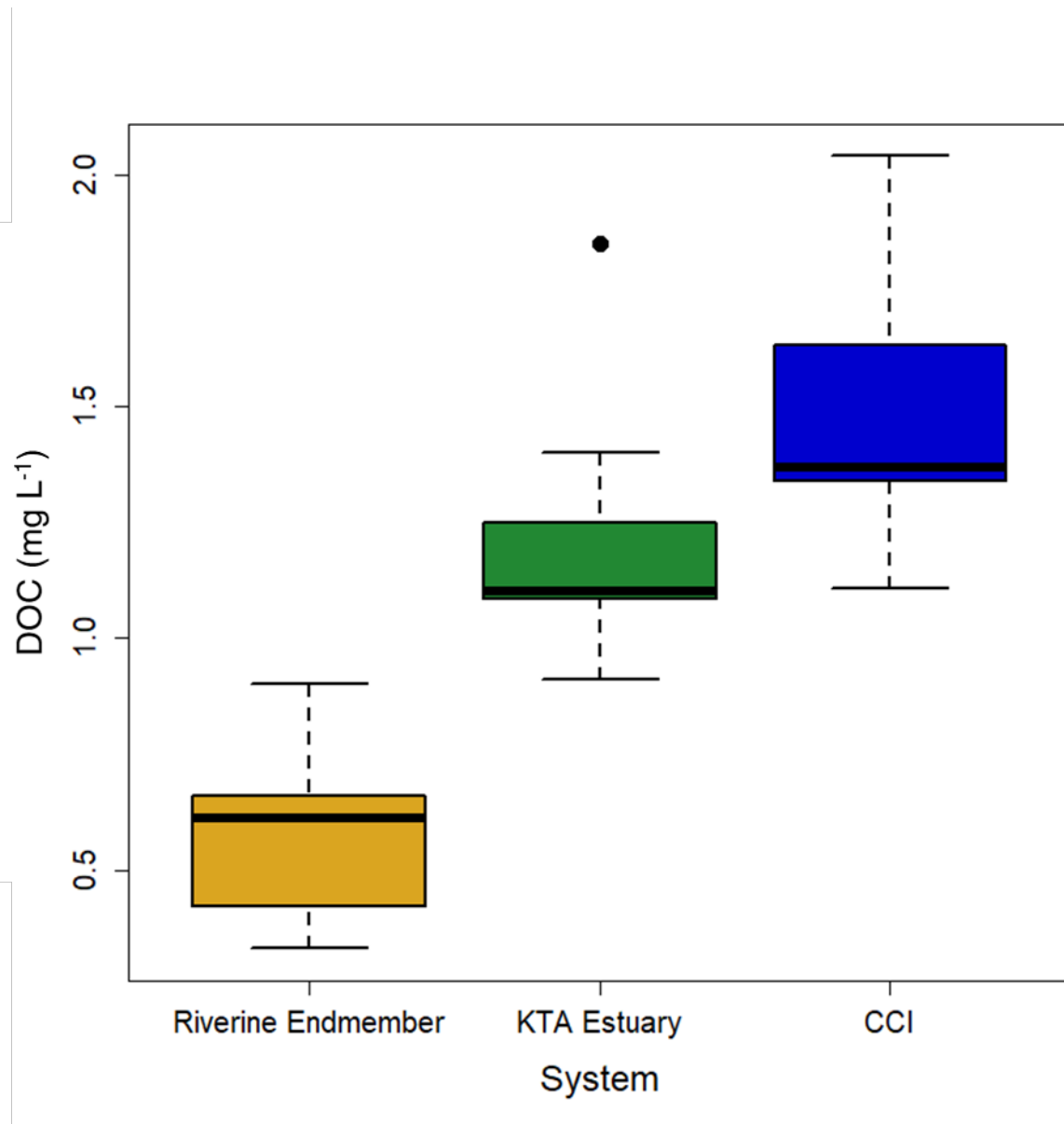


**Figure 12.** Boxplot of DOC in the riverine endmember, the KTA estuary, and the CCI.

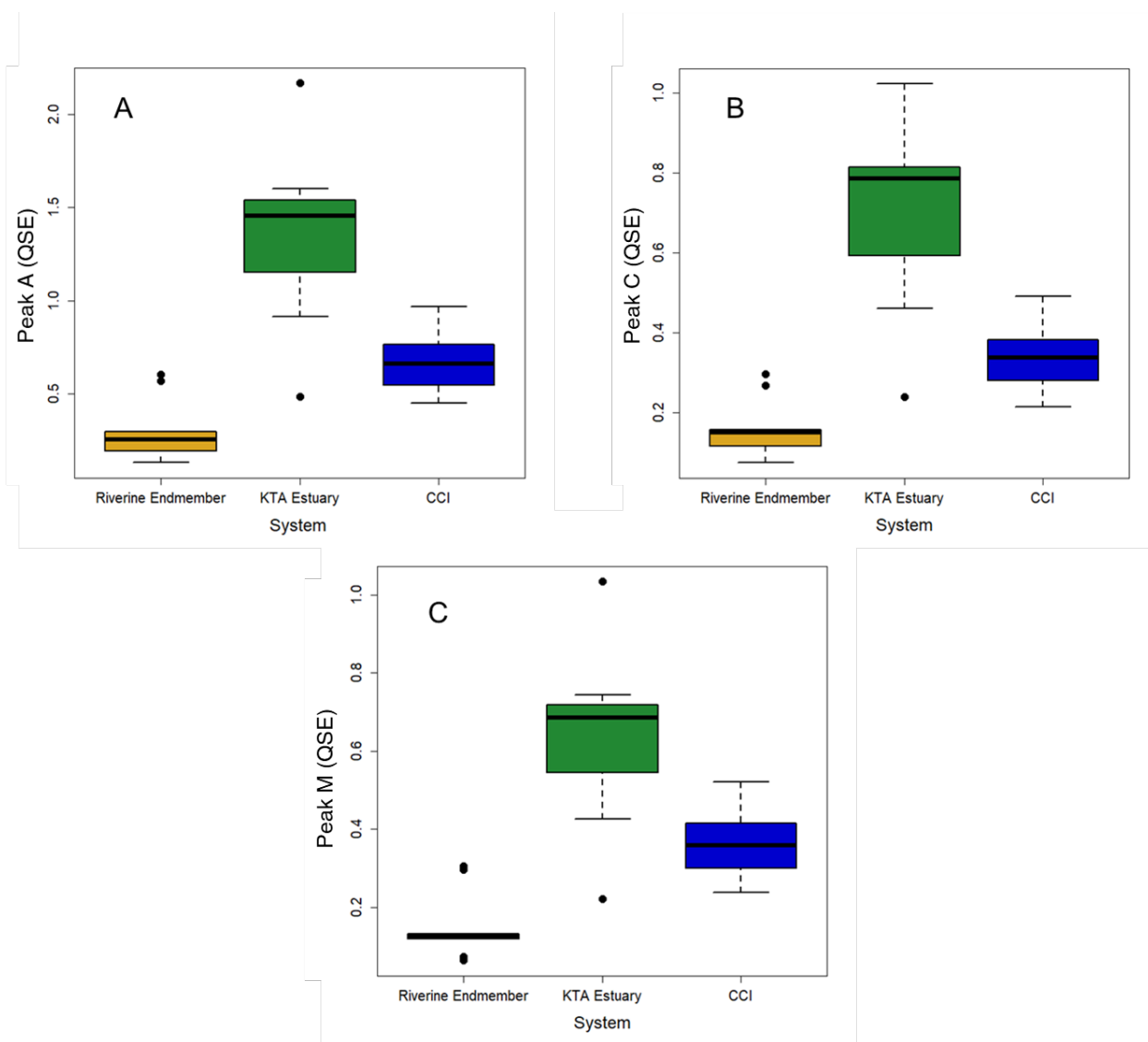


**Figure 13.** Boxplots of humic-like peak A (A), peak C (B), and peak M (C) in the riverine endmember, the KTA estuary, and the CCI.

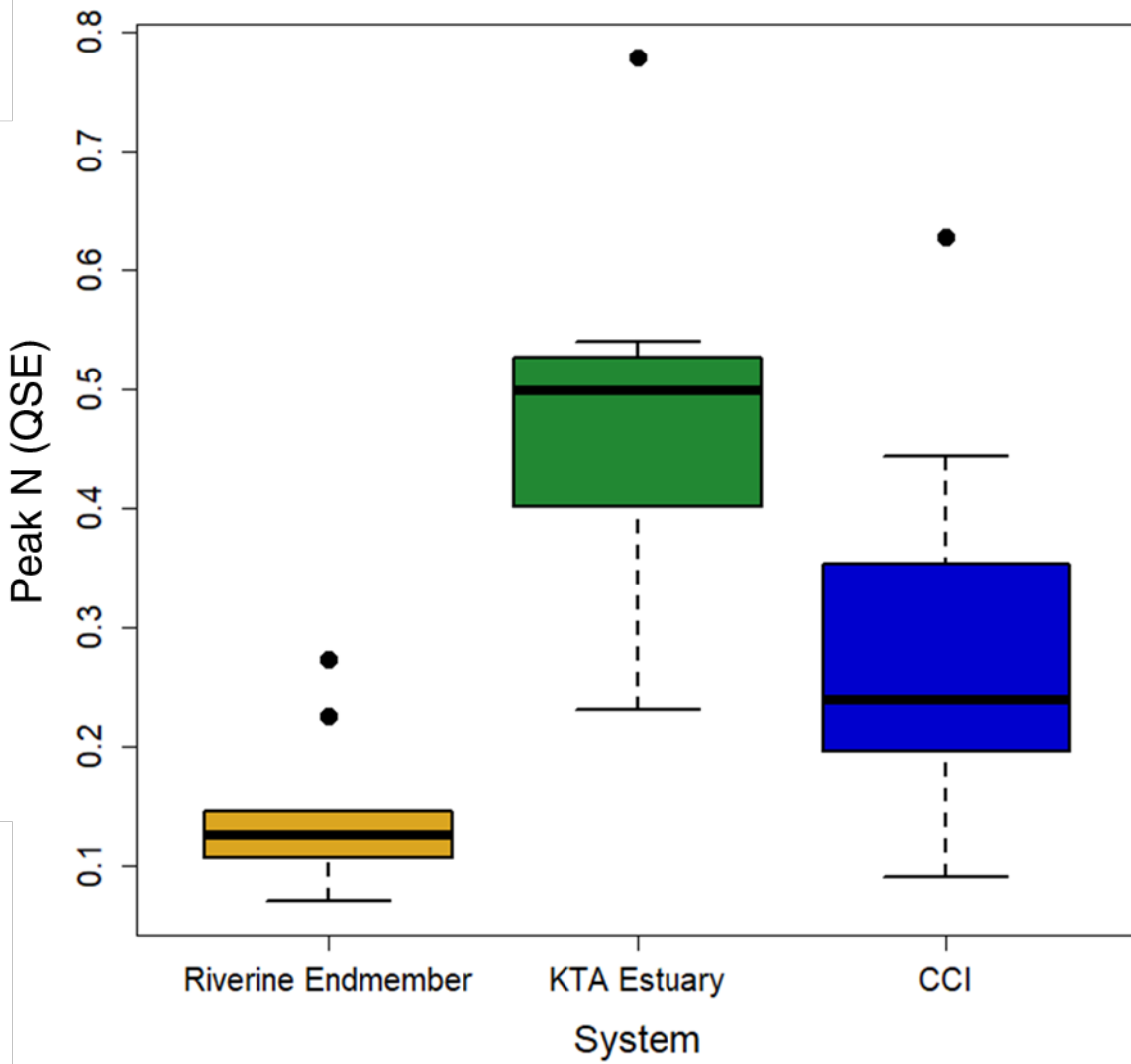


**Figure 14.** Boxplot of peak N in the riverine endmember, the KTA estuary, and the CCI.

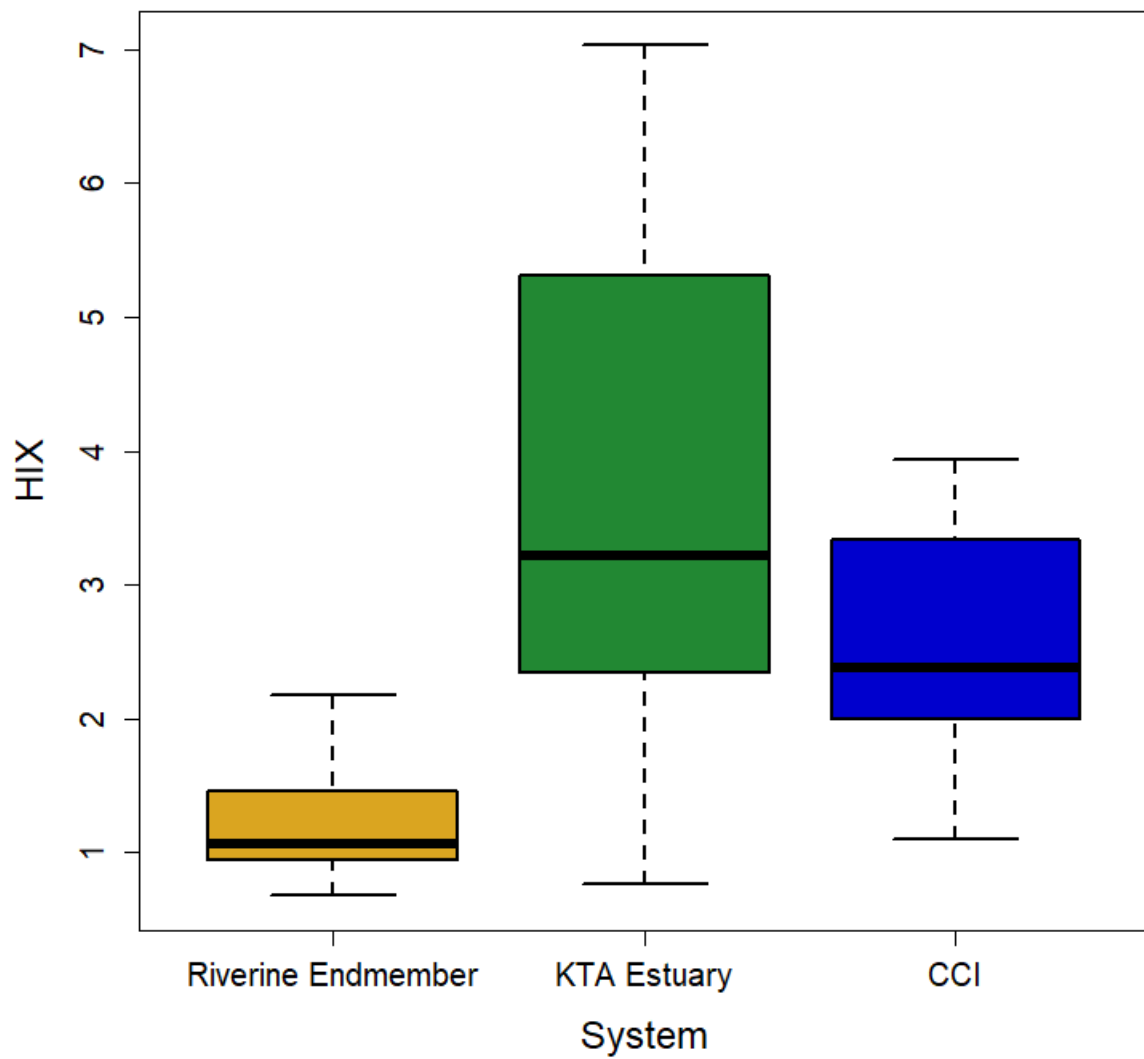


**Figure 15.** Boxplot of HIX for the riverine endmember, the KTA estuary, and the CCI.

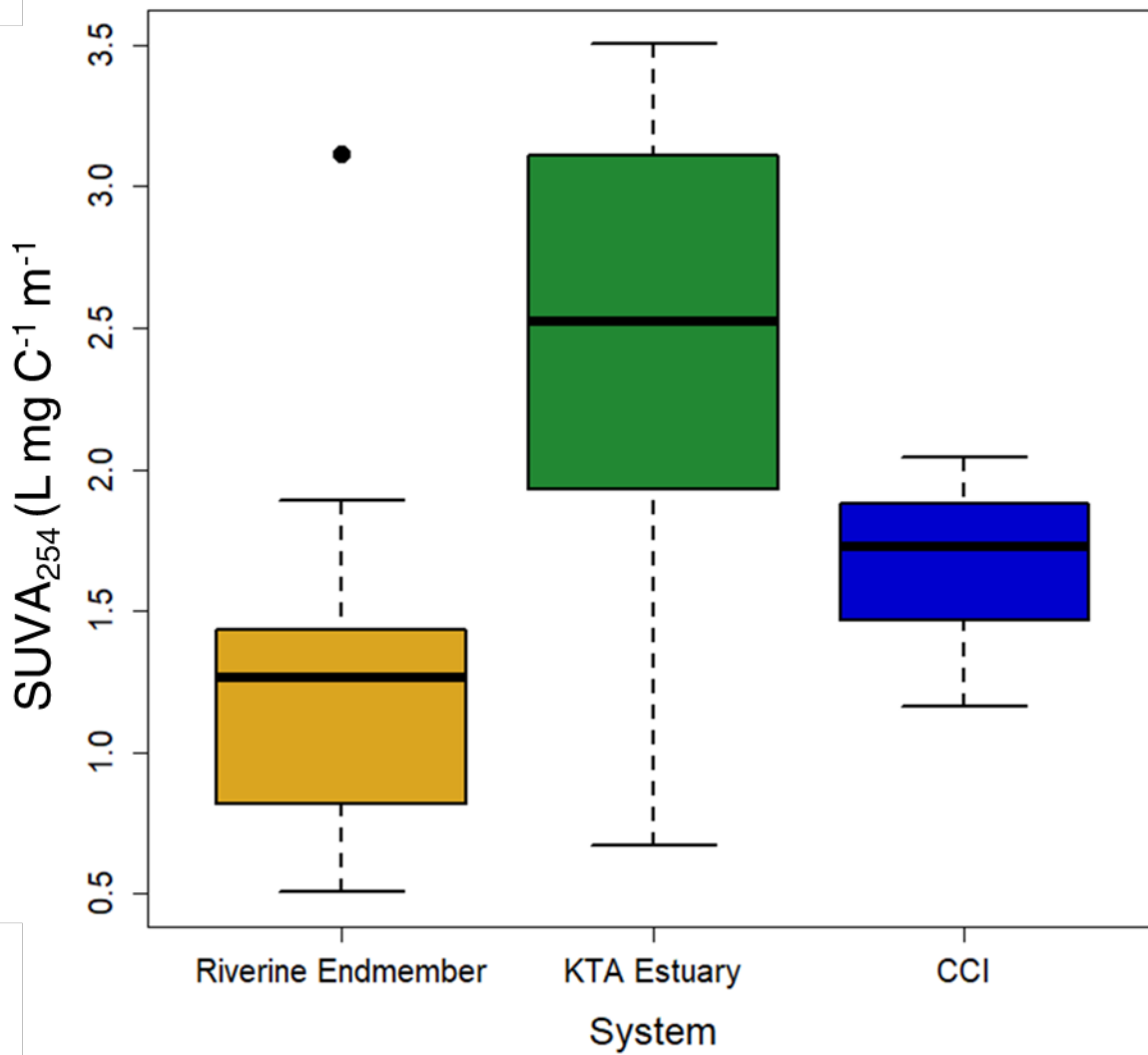


**Figure 16.** Boxplot of SUVA<sub>254</sub> in the riverine endmember, the KTA estuary, and the CCI.

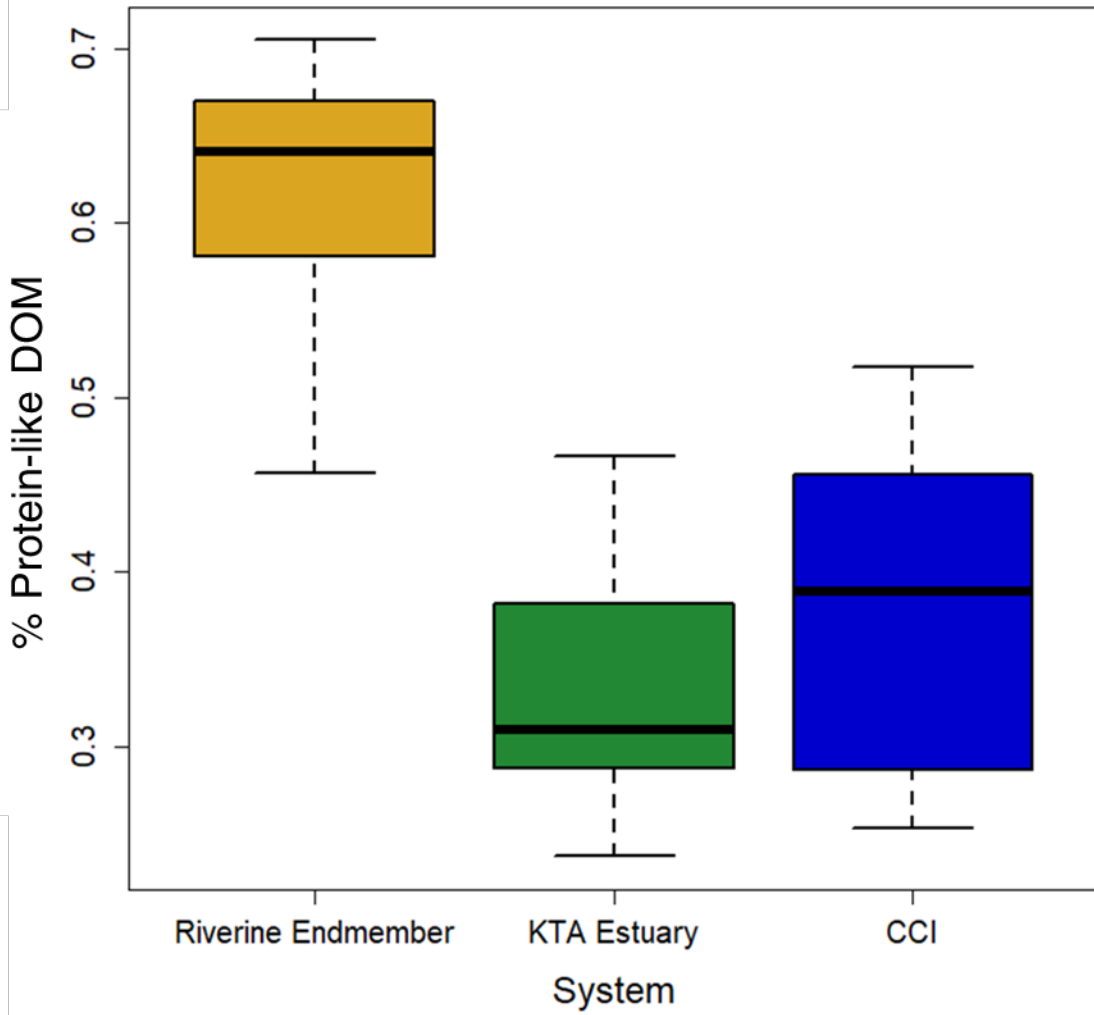


**Figure 17.** Boxplot of %P-DOM for the riverine endmember, the KTA estuary, and the CCI.

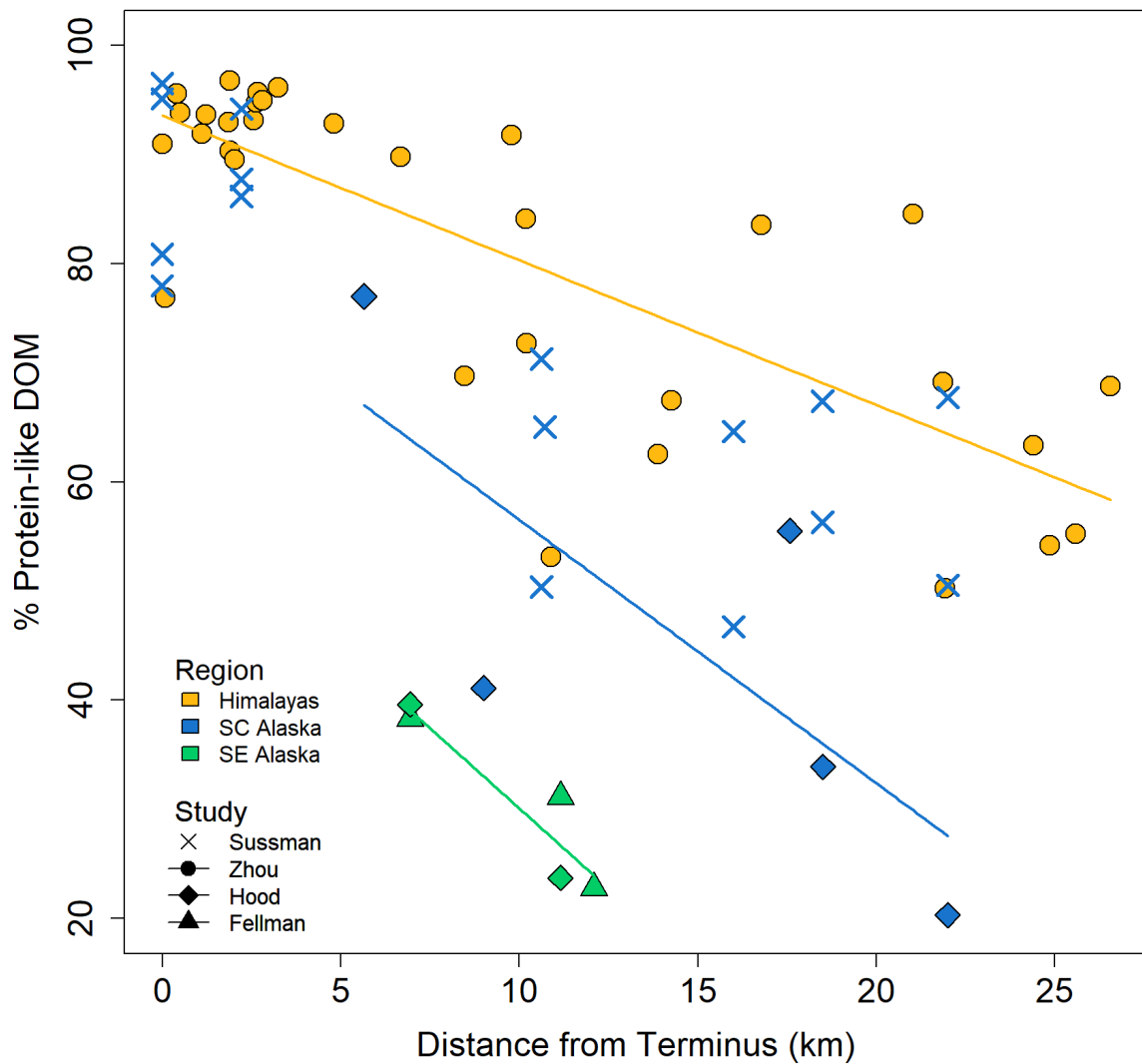


**Figure 18.** Combined %P-DOM versus distance from glacial terminus. Himalayan data from Zhou et al. (2019) is displayed in yellow, combined SC AK original data (x) and data reported in Hood et al. (2009) (diamonds) is displayed in blue, and combined SE AK data from Hood et al. (2009) and Fellman et al. (2010a). Regressions are shown for published data from each region.

## 9.0. REFERENCES

- Alkhatib, M., del Giorgio, P. A., Gelin, Y., & Lehmann, M. F. (2013). Benthic fluxes of dissolved organic nitrogen in the lower St. Lawrence estuary and implications for selective organic matter degradation. *Biogeochemistry*, *10*(11), 7609–7622. <https://doi.org/10.5194/bg-10-7609-2013>
- Alkhatib, M., Jennerjahn, T. C., & Samiaji, J. (2007). Biogeochemistry of the Dumai River estuary, Sumatra, Indonesia, a tropical black-water river. *Limnology and Oceanography*, *52*(6), 2410–2417. <https://doi.org/10.4319/lo.2007.52.6.2410>
- Andrews, J. E., Greenaway, A. M., & Dennis, P. F. (1998). Combined Carbon Isotope and C/N Ratios as Indicators of Source and Fate of Organic Matter in a Poorly Flushed, Tropical Estuary: Hunts Bay, Kingston Harbour, Jamaica. *Estuarine, Coastal and Shelf Science*, *46*(5), 743–756. <https://doi.org/10.1006/ecss.1997.0305>
- Arendt, A. A. (2002). Rapid Wastage of Alaska Glaciers and Their Contribution to Rising Sea Level. *Science*, *297*(5580), 382–386. <https://doi.org/10.1126/science.1072497>
- Arendt, C. A., Aciego, S. M., & Hetland, E. A. (2015). An open source Bayesian Monte Carlo isotope mixing model with applications in Earth surface processes. *Geochemistry, Geophysics, Geosystems*, *16*(5), 1274–1292. <https://doi.org/10.1002/2014GC005683>
- Arimitsu, M. L., Hobson, K. A., Webber, D. N., Piatt, J. F., Hood, E. W., & Fellman, J. B. (2018). Tracing biogeochemical subsidies from glacier runoff into Alaska's coastalmarine food webs. *Global Change Biology*, *24*(1), 387–398. <https://doi.org/10.1111/gcb.13875>
- Barker, J. D., Dubnick, A., Lyons, W. B., & Chin, Y.-P. (2013). Changes in Dissolved Organic Matter (DOM) Fluorescence in Proglacial Antarctic Streams. *Arctic, Antarctic, and Alpine Research*, *45*(3), 305–317. <https://doi.org/10.1657/1938-4246-45.3.305>
- Barker, J. D., Sharp, M. J., Fitzsimons, S. J., & Turner, R. J. (2006). Abundance and Dynamics of Dissolved Organic Carbon in Glacier Systems. *Arctic, Antarctic, and Alpine Research*, *38*(2), 163–172. [https://doi.org/10.1657/1523-0430\(2006\)38\[163:AADODO\]2.0.CO;2](https://doi.org/10.1657/1523-0430(2006)38[163:AADODO]2.0.CO;2)
- Barker, J. D., Sharp, M. J., & Turner, R. J. (2009). Using synchronous fluorescence spectroscopy and principal components analysis to monitor dissolved organic matter dynamics in a glacier system. *Hydrological Processes*, *23*(10), 1487–1500. <https://doi.org/10.1002/hyp.7274>
- Baum, A., Rixen, T., & Samiaji, J. (2007). Relevance of peat draining rivers in central Sumatra

- for the riverine input of dissolved organic carbon into the ocean. *Estuarine, Coastal and Shelf Science*, 73(3), 563–570. <https://doi.org/10.1016/j.ecss.2007.02.012>
- Bhatia, M. P., Das, S. B., Longnecker, K., Charette, M. A., & Kujawinski, E. B. (2010). Molecular characterization of dissolved organic matter associated with the Greenland ice sheet. *Geochimica et Cosmochimica Acta*, 74(13), 3768–3784. <https://doi.org/10.1016/j.gca.2010.03.035>
- Bianchi, T. S. (2007). *Biogeochemistry of Estuaries*. Oxford University Press, USA.
- Boraas, A., & Leggett, A. (2013). Dena'ina Resistance to Russian Hegemony, Late Eighteenth and Nineteenth Centuries: Cook Inlet, Alaska. *Ethnohistory*, 60(3), 485–504. <https://doi.org/10.1215/00141801-2140722>
- Bradner, T. (2015). Dena'ina roots still run deep in Southcentral Alaska. *Alaska Journal of Commerce*, 39(26), 11.
- Brooks, M. L., Meyer, J. S., & McKnight, D. M. (2007). Photooxidation of wetland and riverine dissolved organic matter: Altered copper complexation and organic composition. *Hydrobiologia*, 579(1), 95–113. <https://doi.org/10.1007/s10750-006-0387-6>
- Cawley, K. M., Yamashita, Y., Maie, N., & Jaffé, R. (2014). Using Optical Properties to Quantify Fringe Mangrove Inputs to the Dissolved Organic Matter (DOM) Pool in a Subtropical Estuary. *Estuaries and Coasts*, 37(2), 399–410. <https://doi.org/10.1007/s12237-013-9681-5>
- Cheng, Y., Wang, S., HU, S., ZHOU, C., SHI, Z., LI, Q., & HUANG, X. (2015). The Fluorescence Characteristics of Dissolved Organic Matter (DOM) in the Seagrass Ecosystem from Hainan by Fluorescence Excitation-Emission Matrix Spectroscopy. *Spectroscopy and Spectral Analysis*, 35(1), 141–145. [https://doi.org/10.3964/j.issn.1000-0593\(2015\)01-0141-05](https://doi.org/10.3964/j.issn.1000-0593(2015)01-0141-05)
- Chiffard, P., Fasching, C., Reiss, M., Ditzel, L., & Boodoo, K. S. (2019). Dissolved and Particulate Organic Carbon in Icelandic Proglacial Streams: A First Estimate. *Water*, 11(4), 748. <https://doi.org/10.3390/w11040748>
- Coble, P. G., Del Castillo, C. E., & Avril, B. (1998). Distribution and optical properties of CDOM in the Arabian Sea during the 1995 Southwest Monsoon. *Deep Sea Research Part II: Topical Studies in Oceanography*, 45(10), 2195–2223. [https://doi.org/10.1016/S0967-0645\(98\)00068-X](https://doi.org/10.1016/S0967-0645(98)00068-X)

- Cory, R. M., McKnight, D. M., Chin, Y.-P., Miller, P., & Jaros, C. L. (2007). Chemical characteristics of fulvic acids from Arctic surface waters: Microbial contributions and photochemical transformations. *Journal of Geophysical Research: Biogeosciences*, *112*(G4). <https://doi.org/10.1029/2006JG000343>
- Deboer, D. G. (2009). *Deposition and preservation of estuarine sediment, Turnagain Arm, Cook Inlet, Alaska*. 134.
- Dube, T. (2012). Primary Productivity of Intertidal mudflats in the Wadden Sea: A Remote Sensing Method. *Master's Thesis, University of Twente*, 68.
- Dubnick, A., Barker, J., Sharp, M., Wadham, J., Lis, G., Telling, J., Fitzsimons, S., & Jackson, M. (2010). Characterization of dissolved organic matter (DOM) from glacial environments using total fluorescence spectroscopy and parallel factor analysis. *Annals of Glaciology*, *51*(56), 111–122. <https://doi.org/10.3189/172756411795931912>
- Etherington, L. L., Hooge, P. N., Hooge, E. R., & Hill, D. F. (2007). Oceanography of Glacier Bay, Alaska: Implications for biological patterns in a glacial fjord estuary. *Estuaries and Coasts*, *30*(6), 927–944. <https://doi.org/10.1007/BF02841386>
- Ezer, T., & Liu, H. (2010). On the dynamics and morphology of extensive tidal mudflats: Integrating remote sensing data with an inundation model of Cook Inlet, Alaska. *Ocean Dynamics*, *60*(5), 1307–1318. <https://doi.org/10.1007/s10236-010-0319-x>
- Fellman, J. B., D'Amore, D. V., Hood, E., & Boone, R. D. (2008). Fluorescence characteristics and biodegradability of dissolved organic matter in forest and wetland soils from coastal temperate watersheds in southeast Alaska. *Biogeochemistry*, *88*(2), 169–184. <https://doi.org/10.1007/s10533-008-9203-x>
- Fellman, J. B., Hood, E., Raymond, P. A., Hudson, J., Bozeman, M., & Arimitsu, M. (2015). Evidence for the assimilation of ancient glacier organic carbon in a proglacial streamfood web. *Limnology and Oceanography*, *60*(4), 1118–1128. <https://doi.org/10.1002/lno.10088>
- Fellman, J. B., Hood, E., & Spencer, R. G. M. (2010). Fluorescence spectroscopy opens new windows into dissolved organic matter dynamics in freshwater ecosystems: A review. *Limnology and Oceanography*, *55*(6), 2452–2462. <https://doi.org/10.4319/lo.2010.55.6.2452>
- Fellman, J. B., Hood, E., Spencer, R. G. M., Stubbins, A., & Raymond, P. A. (2014). Watershed

- Glacier Coverage Influences Dissolved Organic Matter Biogeochemistry in Coastal Watersheds of Southeast Alaska. *Ecosystems*, 17(6), 1014–1025.  
<https://doi.org/10.1007/s10021-014-9777-1>
- Fellman, J. B., Petrone, K. C., & Grierson, P. F. (2011). Source, biogeochemical cycling, and fluorescence characteristics of dissolved organic matter in an agro-urban estuary. *Limnology and Oceanography*, 56(1), 243–256. <https://doi.org/10.4319/lo.2011.56.1.0243>
- Fellman, J. B., Spencer, R. G. M., Hernes, P. J., Edwards, R. T., D'Amore, D. V., & Hood, E. (2010). The impact of glacier runoff on the biodegradability and biochemical composition of terrigenous dissolved organic matter in near-shore marine ecosystems. *Marine Chemistry*, 121(1–4), 112–122. <https://doi.org/10.1016/j.marchem.2010.03.009>
- Ford, J., & Bedford, B. L. (1987). The Hydrology of Alaskan Wetlands, U.S.A.: A Review. *Arctic and Alpine Research*, 19(3), 209–229.  
<https://doi.org/10.1080/00040851.1987.12002596>
- Guillemette, F., & Giorgio, P. A. del. (2012). Simultaneous consumption and production of fluorescent dissolved organic matter by lake bacterioplankton. *Environmental Microbiology*, 14(6), 1432–1443. <https://doi.org/10.1111/j.1462-2920.2012.02728.x>
- Hågvar, S., & Ohlson, M. (2013). Ancient carbon from a melting glacier gives high 14 C age in living pioneer invertebrates. *Scientific Reports*, 3(1), 2820.  
<https://doi.org/10.1038/srep02820>
- Hodson, A., Anesio, A. M., Tranter, M., Fountain, A., Osborn, M., Priscu, J., Laybourn-Parry, J., & Sattler, B. (2008). Glacial Ecosystems. *Ecological Monographs*, 78(1), 41–67.  
<https://doi.org/10.1890/07-0187.1>
- Hood, E., Fellman, J., Spencer, R. G. M., Hernes, P. J., Edwards, R., D'Amore, D., & Scott, D. (2009). Glaciers as a source of ancient and labile organic matter to the marine environment. *Nature*, 462(7276), 1044–1047. <https://doi.org/10.1038/nature08580>
- Hood, E., & Scott, D. (2008). Riverine organic matter and nutrients in southeast Alaska affected by glacial coverage. *Nature Geoscience*, 1(9), 583–587. <https://doi.org/10.1038/ngeo280>
- Hotaling, S., Hood, E., & Hamilton, T. L. (2017). Microbial ecology of mountain glacier ecosystems: Biodiversity, ecological connections and implications of a warming climate. *Environmental Microbiology*, 19(8), 2935–2948. <https://doi.org/10.1111/14622920.13766>

- Houghton, J., Starkes, J., & Chambers, M. (2005). *Marine Fish and Benthos Studies—Knik Arm Bridge and Toll Authority*. Yumpu.Com.  
<https://www.yumpu.com/en/document/read/23894682/marine-fish-and-benthos-studies- knik-arm-bridge-and-toll-authority>
- Huguet, A., Vacher, L., Relexans, S., Saubusse, S., Froidefond, J. M., & Parlanti, E. (2009). Properties of fluorescent dissolved organic matter in the Gironde Estuary. *Organic Geochemistry*, 40(6), 706–719. <https://doi.org/10.1016/j.orggeochem.2009.03.002>
- Huss, M., & Hock, R. (2018). Global-scale hydrological response to future glacier mass loss. *Nature Climate Change*, 8(2), 135–140. <https://doi.org/10.1038/s41558-017-0049-x>
- Janet H. Curran & Monica L. McTeague. (2011). *Geomorphology and Bank Erosion of the Matanuska River, Southcentral Alaska* (Scientific Investigations Report) [Scientific Investigations Report]. USGS.
- Kida, M., Kojima, T., Tanabe, Y., Hayashi, K., Kudoh, S., Maie, N., & Fujitake, N. (2019). Origin, distributions, and environmental significance of ubiquitous humic-like fluorophores in Antarctic lakes and streams. *Water Research*, 163, 114901. <https://doi.org/10.1016/j.watres.2019.114901>
- Lamb, A. L., Wilson, G. P., & Leng, M. J. (2006). A review of coastal palaeoclimate and relative sea-level reconstructions using  $\delta^{13}\text{C}$  and C/N ratios in organic material. *Earth-Science Reviews*, 75(1), 29–57. <https://doi.org/10.1016/j.earscirev.2005.10.003>
- Larsen, C. F., Burgess, E., Arendt, A. A., O’Neel, S., Johnson, A. J., & Kienholz, C. (2015). Surface melt dominates Alaska glacier mass balance. *Geophysical Research Letters*, 42(14), 5902–5908. <https://doi.org/10.1002/2015GL064349>
- Manning, D. W. P., Rosemond, A. D., Gulis, V., Benstead, J. P., & Kominoski, J. S. (2018). Nutrients and temperature additively increase stream microbial respiration. *Global Change Biology*, 24(1), e233–e247. <https://doi.org/10.1111/gcb.13906>
- Milner, A. M., Khamis, K., Battin, T. J., Brittain, J. E., Barrand, N. E., Füreder, L., Cauvy-Fraunié, S., Gíslason, G. M., Jacobsen, D., Hannah, D. M., Hodson, A. J., Hood, E., Lencioni, V., Ólafsson, J. S., Robinson, C. T., Tranter, M., & Brown, L. E. (2017). Glacier shrinkage driving global changes in downstream systems. *Proceedings of the National Academy of Sciences*, 114(37), 9770–9778. <https://doi.org/10.1073/pnas.1619807114>

- Molchan-Douthit, M. (1998). Alaska bore tales. *National Oceanic and Atmospheric Administration*.
- Molnia, B. F. (2008). Glaciers of North America—Glaciers of Alaska. In *Glaciers of North America—Glaciers of Alaska* (USGS Numbered Series No. 1386-K; Professional Paper, Vols. 1386-K). Geological Survey (U.S.). <https://doi.org/10.3133/pp1386K>
- Moody, C. S., & Worrall, F. (2017). Modeling rates of DOC degradation using DOM composition and hydroclimatic variables. *Journal of Geophysical Research: Biogeosciences*, *122*(5), 1175–1191. <https://doi.org/10.1002/2016JG003493>
- Neal, E. G., Hood, E., & Smikrud, K. (2010). Contribution of glacier runoff to freshwater discharge into the Gulf of Alaska. *Geophysical Research Letters*, *37*(6). <https://doi.org/10.1029/2010GL042385>
- Oey, L.-Y., Ezer, T., Hu, C., & Muller-Karger, F. E. (2007). Baroclinic tidal flows and inundation processes in Cook Inlet, Alaska: Numerical modeling and satellite observations. *Ocean Dynamics*, *57*(3), 205–221. <https://doi.org/10.1007/s10236-007-0103-8>
- Opsahl, S. P. (2005). Organic Carbon Composition and Oxygen Metabolism across a Gradient of Seasonally Inundated Limesink and Riparian Wetlands in the Southeast Coastal Plain, USA. *Biogeochemistry*, *76*(1), 47–68. <https://doi.org/10.1007/s10533-005-2074-5>
- Osburn, C. L., & Morris, D. P. (2003). Photochemistry of chromophoric dissolved organic matter in natural waters. 1, 185–217. In *UV effects in aquatic organisms and ecosystems* (pp. 185–217).
- Osburn, C. L., & St-Jean, G. (2007). The use of wet chemical oxidation with high-amplification isotope ratio mass spectrometry (WCO-IRMS) to measure stable isotope values of dissolved organic carbon in seawater. *Limnology and Oceanography: Methods*, *5*(10), 296–308. <https://doi.org/10.4319/lom.2007.5.296>
- Powers, S. P., Bishop, M. A., & Clesceri, E. (2005). *Characterization of Energy and Potential Contaminant Pathways in Subarctic Estuarine Habitats: Ecology of Tidal Flat Communities of the Copper River Delta, Alaska*. 25.
- Powers, S. P., Bishop, M. A., Grabowski, J. H., & Peterson, C. H. (2002). Intertidal benthic resources of the Copper River Delta, Alaska, USA. *Journal of Sea Research*, *47*(1), 13–23. [https://doi.org/10.1016/S1385-1101\(01\)00102-2](https://doi.org/10.1016/S1385-1101(01)00102-2)

- Raymond, P. A., & Bauer, J. E. (2001). DOC cycling in a temperate estuary: A mass balance approach using natural  $^{14}\text{C}$  and  $^{13}\text{C}$  isotopes. *Limnology and Oceanography*, 46(3), 655–667. <https://doi.org/10.4319/lo.2001.46.3.0655>
- Reed, J. C., & Harms, J. C. (1956). Rates of Tree Growth and Forest Succession in the Anchorage-Matanuska Valley Area, Alaska. *Arctic* 9(4), 238-248. <https://doi.org/10.14430/arctic3798>
- Ren, Z., Gao, H., & Elser, J. J. (2017). Longitudinal variation of microbial communities in benthic biofilms and association with hydrological and physicochemical conditions in glacier-fed streams. *Freshwater Science*, 36(3), 479–490. <https://doi.org/10.1086/693133>
- Ren, Z., Martyniuk, N., Oleksy, I. A., Swain, A., & Hotaling, S. (2019). Ecological Stoichiometry of the Mountain Cryosphere. *Frontiers in Ecology and Evolution*, 7. <https://doi.org/10.3389/fevo.2019.00360>
- Rudolph, J. C., Arendt, C. A., Hounshell, A. G., Paerl, H. W., & Osburn, C. L. (2020). Use of Geospatial, Hydrologic, and Geochemical Modeling to Determine the Influence of Wetland-Derived Organic Matter in Coastal Waters in Response to Extreme Weather Events. *Frontiers in Marine Science*, 0. <https://doi.org/10.3389/fmars.2020.00018>
- Singer, G. A., Fasching, C., Wilhelm, L., Niggemann, J., Steier, P., Dittmar, T., & Battin, T. J. (2012). Biogeochemically diverse organic matter in Alpine glaciers and its downstream fate. *Nature Geoscience*, 5(10), 710–714. <https://doi.org/10.1038/ngeo1581>
- Strom, S. L., Fredrickson, K. A., & Bright, K. J. (2016). Spring phytoplankton in the eastern coastal Gulf of Alaska: Photosynthesis and production during high and low bloom years. *Deep Sea Research Part II: Topical Studies in Oceanography*, 132, 107–121. <https://doi.org/10.1016/j.dsr2.2015.05.003>
- Stubbins, A., Hood, E., Raymond, P. A., Aiken, G. R., Sleighter, R. L., Hernes, P. J., Butman, D., Hatcher, P. G., Striegl, R. G., Schuster, P., Abdulla, H. A. N., Vermilyea, A. W., Scott, D. T., & Spencer, R. G. M. (2012). Anthropogenic aerosols as a source of ancient dissolved organic matter in glaciers. *Nature Geoscience*, 5(3), 198–201. <https://doi.org/10.1038/ngeo1403>
- Telling, J., Anesio, A. M., Hawkings, J., Tranter, M., Wadham, J. L., Hodson, A. J., Irvine-Fynn, T., & Yallop, M. L. (2010). Measuring rates of gross photosynthesis and net community production in cryoconite holes: A comparison of field methods. *Annals of Glaciology*,

51(56), 153–162. <https://doi.org/10.3189/172756411795932056>

Weishaar, J. L., Aiken, G. R., Bergamaschi, B. A., Fram, M. S., Fujii, R., & Mopper, K. (2003).

Evaluation of Specific Ultraviolet Absorbance as an Indicator of the Chemical Composition and Reactivity of Dissolved Organic Carbon. *Environmental Science & Technology*, 37(20), 4702–4708. <https://doi.org/10.1021/es030360x>

Yamashita, Y., Panton, A., Mahaffey, C., & Jaffé, R. (2011). Assessing the spatial and temporal variability of dissolved organic matter in Liverpool Bay using excitation–emission matrix fluorescence and parallel factor analysis. *Ocean Dynamics*, 61(5), 569–579.

<https://doi.org/10.1007/s10236-010-0365-4>

Zhou, Y., Zhou, L., He, X., Jang, K.-S., Yao, X., Hu, Y., Zhang, Y., Li, X., Spencer, R. G. M.,

Brookes, J. D., & Jeppesen, E. (2019). Variability in Dissolved Organic Matter Composition and Biolability across Gradients of Glacial Coverage and Distance from Glacial Terminus on the Tibetan Plateau. *Environmental Science & Technology*, 53(21), 12207–12217. <https://doi.org/10.1021/acs.est.9b03348>